Curr Pollution Rep (2015) 1:95–116
DOI 10.1007/s40726-015-0010-4

AIR POLLUTION (S WU, SECTION EDITOR)

Sources and Impacts of Atmospheric NH_3: Current Understanding and Frontiers for Modeling, Measurements, and Remote Sensing in North America

Liye Zhu[1,2] · Daven K. Henze[1] · Jesse O. Bash[3] · Karen E. Cady-Pereira[4] · Mark W. Shephard[5] · Ming Luo[6] · Shannon L. Capps[1,3]

Published online: 11 August 2015

Abstract Ammonia (NH_3) contributes to widespread adverse health impacts, affects the climate forcing of ambient aerosols, and is a significant component of reactive nitrogen, deposition of which threatens many sensitive ecosystems. Historically, the scarcity of in situ measurements and the complexity of gas-to-aerosol NH_3 partitioning have contributed to large uncertainties in our knowledge of its sources and distributions. However, recent progress in measurements and modeling has afforded new opportunities for improving our understanding of NH_3 and the role it plays in these important environmental issues. In the past few years, passive measurements of NH_3 have been added to monitoring networks throughout the USA, now in place at more than 60 stations, while mobile measurements aboard aircrafts and vehicles have provide detailed observations during several recent field campaigns. In addition, new remote sensing observations from multiple satellite instruments have begun to provide vast amounts of NH_3 observations throughout the globe. These sources of information have collectively driven new air quality modeling capabilities, by revealing deficiencies in current air quality models and spurring development of mechanistic enhancements to models' physical representation of the diurnal variability and bidirectional nature of NH_3 fluxes. In turn, these advanced models require further observational constraints, as existing NH_3 measurements are still limited in spatiotemporal coverage. We thus evaluate the potential value of a new geostationary remote sensing instrument (GCIRI) for providing constraints on NH_3 fluxes through multiple Observing System Simulation Experiments (OSSEs).

Keywords Ammonia · North America · Sources and impacts · Measurements techniques · Low-earth-orbit and geostationary remote sensing · Diurnal variability · Bidirectional exchange

This article is part of the Topical Collection on *Air Pollution*

✉ Daven K. Henze
daven.henze@colorado.edu

1 Department of Mechanical Engineering, University of Colorado, Boulder, CO, USA

2 Department of Atmospheric Science, Colorado State University, Fort Collins, CO, USA

3 US Environmental Protection Agency, Research Triangle Park, Durham, NC, USA

4 Atmospheric and Environmental Research, Inc., Lexington, MA, USA

5 Environment Canada, Toronto, Ontario, Canada

6 Jet Propulsion Laboratory, California Institute of Technology, Pasadena, CA, USA

Introduction

The nitrogen in ammonia (NH_3) is an important component of the global nitrogen cycle, which plays an important role in every ecosystem. While by itself NH_3 has a residence time in the atmosphere of only a day or less, it contributes to the formation of atmospheric aerosols that reside in the atmosphere for several days to a week [64, 127, 130, 178]. NH_3 is thus responsible for a significant fraction of the long-range transport (hundreds of kilometer) of reactive nitrogen [62]. However, the natural nitrogen cycle has shifted dramatically in recent decades due to human

activities. Widespread dispersion, transport, and deposition of NH_3 through the atmosphere contribute to a number of environmental and human health concerns. Largely unregulated emissions of NH_3 from anthropogenic actives have increased several folds since pre-industrial times, and they are the only such sources of ambient aerosol particles whose emissions are projected to rise, globally, throughout the next century [113]. Compared to measurement capabilities for other aerosol precursors or sources of reactive nitrogen, observations of NH_3 have been sparse until recent years. This historical lack of data has contributed to large uncertainties in our present understanding of the role NH_3 plays in the nexus of air quality, climate, ecosystems, and food security.

Here, we review current knowledge of atmospheric NH_3, beginning with an overview of NH_3 sources (Section "Sources of NH_3") and the impacts of NH_3 on human health and the environment (Section "Impacts of Atmospheric NH_3"). We next review current measurements techniques for NH_3, from both passive and active in situ observations to new remote sensing techniques. Lastly, we consider the value of a recently proposed geostationary remote sensing instrument (GCIRI) that would provide the first geostationary measurements of NH_3 over North America. Given the state of knowledge of NH_3, we conclude that the potential of such an instrument to enhance our understanding of NH_3 sources and distributions at a mechanistic level could significantly improve our ability to treat NH_3 in chemistry and climate models, thereby increasing the value of such tools for environmental decision-making.

Sources of NH_3

The primary source of global NH_3 emissions is agriculture (~85 %), which includes NH_3 emissions from livestock and NH_3-based fertilizer applications. Other sources of NH_3 emissions include industrial processes, motor vehicles, plant decomposition, biomass burning, and volatilization from soils and oceans. Early nitrogen cycle studies estimated that NH_3 emissions contribute ~75 Tg N year^{-1} of the global N budget (~250 Tg year^{-1}) [152]. Global emission inventories were subsequently developed [21, 42]; however, owing to the lack of NH_3 measurements in most regions of the globe, such estimates were hard to evaluate and contained large uncertainties. For example, the global estimate of NH_3 emissions is 54 Tg N year^{-1} with 25 % uncertainty in Bouwman et al. [21], which is lower than 75 Tg N year^{-1} (with potential range from 50 to 128 Tg N year^{-1}) of Schlesinger and Hartley [152] and somewhat higher than 45 Tg N year^{-1} with 50 % uncertainty by Dentener and Crutzen [42]. More recently, the Emissions Database for Global Atmospheric Research (EDGAR) compiled NH_3 anthropogenic emissions for the past and present day, and Beusen et al. [19] derived a global inventory of NH_3 emissions from agriculture with 0.08° × 0.08° resolution for 2000. A new global, monthly, emission inventory, Magnitude And Seasonality of Agricultural Emissions for NH_3 (MASAGE_NH3), was developed based on the worldwide emission estimates on regional agricultural activities [130]. In addition to global emissions estimates, there are numerous studies on regional NH_3 emissions, for example, in China [79, 165, 189], the USA [65, 66, 127, 134], India [5], Europe [58, 160, 161], France [71], and Canada [174]. Summaries of some of these inventories are included in Table 1.

Recent studies have indicated that global emissions of NH_3 have already increased by a factor of two to five since pre-industrial times [94], following increases in the demand for food for growing populations, especially for increasing agriculture activities in developing countries [4, 38, 49]. Global emissions of NH_3 are projected to continue to rise over the next 100 years in all Representative Concentration Pathways (RCPs) [113]. The projected anthropogenic emissions of NH_3 are estimated to double by 2100 in RCP2.6 and RCP 8.5 (67 Tg N year^{-1}) and increase the least in RCP4.5 (43.6 Tg N year^{-1}) relative to year 2000 estimates of 38.5 Tg N year^{-1} [142]. While such projections have yet to be widely evaluated, in some regions, NH_3 emissions have and are expected to continue to decline, such as in the EU, where a 26 % reduction was found in EEA-33 (33 member countries of European Environment Agency) NH_3 emissions from agricultural between the years 1990 and 2011 [44], mainly due to reduced livestock and improved handling and management of manure. Although NH_3 emissions are generally from agricultural productions, NH_3 fluxes are extremely climate-sensitive [169]. The NH_3 volatilization potential could double every 5° K. NH_3 could also be absorbed by organisms through decomposition associated with water availability. Thus, for future NH_3 emission estimates, further attention should be paid to the impact of climate change, interaction of the vegetation canopy and soil wetness, agricultural management practices, and land use changes.

Developing NH_3 emission inventories such as those discussed above is challenging in many aspects owing to uncertainties in management practices (i.e., activity data), emission factors, and variability at different temporal scales. There are several approaches to building emissions inventories. "Bottom-up" emission inventories are built from spatial and temporal information of the emission sources and source-specific emission factors (e.g., [12, 130, 133, 134]). This requires a detailed knowledge of climate conditions and farming practices, or detailed reporting practices, which may not be readily available. In

Table 1 Summary of global and regional NH_3 emission estimates in teragram N per year

Source	Global	North America	Contiguous US	Spatial resolution	Year
Total					
Schlesinger and Hartley [152]	75	[a]			1990
Dentener and Crutzen [42]	45	5.2[b]		10° × 10°	1990
Bouwman et al. [21]	54	3.6		1° × 1°	1990
EDGAR v4.2	40.6	4.1	2.9	1° × 1°	2008
Moss et al. [113]	38.5	5.1	3.4	0.5° × 0.5°	2000
Moss et al. [113][d]	46.4–58.4	6.5–7.7	4.5–5.0	0.5° × 0.5°	2050
Livestock and fertilizer					
Beusen et al. [19]	32		2.1[c]	0.08° × 0.08°	2000
Paulot et al. [130]	54	3.1	2.7	0.5° × 0.5°	2005–2008
US National Emissions Inventory 2005			3.1	4×4 km^2	2005

[a]Data not available

[b]North and Central America (including anthropogenic, wild animals, and vegetation)

[c]Livestock operations only (including manure spreading and excluding fertilizer use)

[d]Ranges span the RCP 4.5 to RCP 8.5 estimates, which had the widest range of global values across all RCPs in 2050

contrast, inverse modeling approaches generate "top-down" emission estimates by optimizing model predictions in order to match the available observations from in situ monitoring sites [65, 66, 77, 130, 187] and remote sensing [190]. Ultimately, both approaches are required.

Impacts of Atmospheric NH_3

Atmospheric NH_3 readily condenses onto sulfuric acid and with nitric acid to form what is often a ternary mixture of sulfate (SO_4^{2-}), ammonium (NH_4^+), and nitrate (NO_3^-) in water, which commonly contains salts such as ammonium sulfate ($(NH_4)_2SO_4$) and ammonium nitrate (NH_4NO_3). Uptake of nitric acid to form NO_3^- is largely controlled by the presence of NH_3 concentrations in excess of the amount required to neutralize sulfate; thus, aerosol nitrate (NO_3^-) is often considered a byproduct of NH_3. The presence of NH_3 can also play a role in the formation of secondary organic aerosol (SOA) via processes such as ozonolysis of α-pinene through condensation of organic salts [116], although an impact on SOA from oxidation of other species such as isoprene has not been found [104]. In turn, pre-existing organic aerosol may also impact NH_3 uptake (e.g., [20, 96, 102, 106, 171]). NH_3 also contributes to new particle formation through ternary homogenous nucleation, multicomponent nucleation, and ion-induced nucleation (e.g., [9, 68, 89, 93, 117, 162]).

Philip et al. [131] synthesized the remote sensing observations and global model simulations to estimate that ammonium, sulfate, and nitrate constitute about a third of the global average population-weighted fine particulate matter (particles with aerodynamic diameter less than 2.5 μm, i.e., $PM_{2.5}$) concentration of 37 $\mu g\ m^{-3}$, with NH_4^+ contributing 2.7 ± 1.2 $\mu g\ m^{-3}$. Surface-based composition measurements using aerosol mass spectrometers (AMS) in urban areas worldwide consistently report Northern Hemisphere urban PM_1 concentration fractions (excluding dust) of 14, 18, and 23 % for ammonium, nitrate, and sulfate [188]. These are consistent with the composition breakdown from Philip et al. [131], considering that the latter includes a 30 % contribution from mineral dust. In contrast to background concentrations, driven primarily by agricultural sources, episodic pollution events in urban locations such as New York and Beijing are often significantly influenced by traffic emissions [70, 149] even though these are a small fraction of total global emissions.

The contribution of ammonia to $PM_{2.5}$ poses significant health concerns. Numerous studies have shown that exposure to $PM_{2.5}$ is associated with a range deleterious impacts on human health, such as increased hospital admissions, cardiovascular, respiratory, and all-cause mortality [24, 36, 98, 140, 141, 146, 153]. Exposure to ambient air pollution is ranked as one of the top ten risk factors for mortality worldwide [103], annually causing an estimated 3 million premature deaths globally [23] and more than 100,000 premature deaths in the USA alone [51]. While NH_4^+ and NO_3^- may have health impacts unique from those of total $PM_{2.5}$ mass (e.g., [16, 26, 99]), most current air quality policies rely upon well established relationships between total $PM_{2.5}$ mass and health [27, 48].

While NH_3 is not the largest contributor to $PM_{2.5}$, the response of human health impacts to changes in NH_3 can be quite significant, owing to the highly nonlinear relationship between ambient NH_3 concentrations and the formation of

ammonium nitrate. Several studies have shown that the most efficient control of $PM_{2.5}$ is often NH_3 emissions [77, 127, 135, 175, 184], owing to NH_3 concentrations controlling ammonium nitrate concentrations, especially in winter, with notable exceptions being regions with consistently elevated NH_3 concentrations such as India [86]. Recent studies have attempted to evaluate the economic or health impact per unit emission of NH_3, i.e., the marginal damages of NH_3 emissions (e.g., [69, 167]). For example, using a combination of remote sensing and adjoint sensitivity analysis, Lee et al. [97] evaluated the contribution of aerosol and aerosol precursor emissions to global premature deaths. They found that for a 1 kg km^{-2} $year^{-1}$ reduction of any $PM_{2.5}$ precursor emission, anywhere in the world, the largest reduction in global prematures death occurred for NH_3 emissions in Europe [97], with damages of up to 15 premature deaths per kilogram (km^{-2} $year^{-1}$). Fann et al. [50] estimated monetized damages (using a statistical value of life of US$6 million) of US$38,000 and US$95,000 per ton of NH_3 emitted from area and mobile sources, respectively, averaged across nine urban areas within the USA. Dedoussi and Barrett [37] used adjoint sensitivity analysis to estimate the spatial, sectoral, and seasonal impact of NH_3 emissions on premature deaths in the USA, finding that urban NH_3 emissions had ~20 times as large the damages of NO_x per ton of emission. Paulot and Jacob [128] estimated that the damages from agricultural emissions of NH_3 for food export alone contributed to US$36 billion annually from premature deaths in the USA. Buonocore et al. [25] estimated that power plant emissions in the USA lead to US$16,000 in damages per ton of NO_x emissions, 34 % of which is owing to formation of ammonium nitrate. These responses may be overestimated in models that do not include the uptake of nitrate on sea salt [7]. They also do not consider the potential role of NH_3 in terms of particle acidity [81] and its impact on secondary organic aerosol formation (e.g., [82]), although verifying such mechanisms in ambient conditions has been elusive (e.g., [104]). Nevertheless, many models used for evaluation of air quality control strategies may still underestimate the response of $PM_{2.5}$ to ammonia reductions [18].

Along with its impact on air quality, NH_3 can have significant impacts on climate. Ammonium sulfate and ammonium nitrate aerosol scatter incoming solar radiation, which causes a negative direct radiative forcing (i.e., cooling effect). Early estimates of the pre-industrial to present day ammonium aerosol direct radiative forcing crudely accounted for ammonium via spatially uniform ratios applied to prognostic estimates of aerosol sulfate to represent neutralization by ammonium (e.g., [30, 54, 74, 75]). The first direct global simulation of ammonium nitrate to include spatially heterogenous thermodynamic calculations [2] was used to estimate a nitrate aerosol direct radiative forcing of -0.2 W m^{-2} since pre-industrial times [3]. The overall magnitude of this forcing has been refined by subsequent individual global modeling estimates (e.g., [13, 17, 73, 78, 83, 101, 114, 158, 186]); multi-model assessments have ranged from -0.10 ± 0.04 W m^{-2} [115] to -0.19 ± 0.18 W m^{-2} [159], and in situ measurements have confirmed large regional contributions of ammonium nitrate to total aerosol extinction near large agricultural NH_3 sources [95]. While NH_3 is not the largest contributor to the total pre-industrial to present aerosol radiative forcing estimate of -0.5 ± 4 W m^{-2} [115], box model calculations [183] and global model sensitivity studies [78] have shown that NH_3 has the largest aerosol direct radiative forcing efficiency (W m^{-2} per kg of emission) of all aerosol and aerosol precursor emissions. The impact of NH_3 on climate will therefore likely become even more pronounced as sulfate concentrations decrease in regions with low SO_2 emissions [112]. Projections of future radiative forcing thus include large effects of NH_3 (up to -0.15 Wm^{-2} by 2050) via enhanced direct radiative forcing of ammonium nitrate [3, 13, 73, 78, 101], emphasizing the importance of NH_3 as the role of other species declines [163].

In addition to impacting direct radiative forcing by contributing to the mass concentrations of ammonium nitrate and ammonium sulfate, NH_3 contributes to climate by multiple indirect mechanisms. The presence of ammonium can impact aerosol radiative forcing by influencing the phase of secondary inorganic aerosol [180], which modulates aerosol direct radiative forcing by ~25 % globally, with larger variations regionally [109, 181]. There is also a growing body of literature indicating that NH_3 enhances the light-absorbing properties of organic aerosol (e.g., [20, 171]), a mechanism by which increasing NH_3 emissions would exert a positive radiative forcing. Ammonium sulfate also enhances (relative to sulfate alone) indirect aerosol radiative forcing through heterogeneous ice nucleation [1]. Enhanced nitrate concentrations over large NH_3 sources have been observed to contribute to activation of cloud condensation nucleii (CCN) [164]. The contribution of NH_3 to the deposition of reactive nitrogen has been estimated to induce a negative climate forcing by altering carbon fluxes that is similar in magnitude to the direct aerosol radiative forcing of ammonium nitrate itself [137, 138], a larger effect than previously recognized [145].

In addition to the impact of NH_3 on human health and the environment from aerosol formation, the contribution of anthropogenic NH_3 to reactive nitrogen deposition in the form of NH_3 and NH_4^+ (and associated NO_3^-) impacts the nitrogen cascade [57, 60, 63] and poses a threat to sensitive ecosystems [84, 92, 176]. Excessive deposition of NH_3 causes eutrophication in surface water and soil acidification (e.g., [28, 43, 126, 132, 168]) and can further cause nutrient imbalances in sensitive ecosystems [105].

Levels of reactive nitrogen deposition exceed those deemed critical for the protection of biodiversity in many regions throughout the USA [47] and the world [41, 129], now or in the next few decades, underscoring concerns not only of past but also future impacts of anthropogenic activity on the global nitrogen cycle [22, 61, 62, 151]. Despite the recognized importance of this issue, uncertainties in our ability to model such processes may hinder efforts in the USA to develop secondary air quality standards to protect ecosystems from the hazards of this type of pollutant deposition [90].

Current Observations of NH_3 in North America

In Situ Measurements

The measurement of ambient NH_3 is difficult due to the tendency of the small, polar gas molecule to adhere to instrument surfaces or to volatilize from passive samplers. As with other in situ observations, techniques used to evaluate atmospheric ammonia range from simpler approaches deployed broadly to more highly resolved measurements used in specific field campaigns. A summary of techniques employed in North America is provided in Table 2. The largest scale measurements are taken through the National Atmospheric Deposition Program (NADP), which prototyped the Ammonia Monitoring Network (AMoN) in 2007 and then launched a full-fledged network in 2010 in order to establish continuous records of atmospheric NH_3 concentrations (http://nadp.sws.uiuc.edu/amon). Currently, at more than 60 sites nationwide, AMoN provides 2-week integrated samples of ammonia using Radiello® passive sampling devices that contain phosphoric acid in the filter to ensure absorption of ammonia [144]. Although other passive samplers performed similarly to this instrument in a year-long intercomparison, the ease of sample preparation led the NADP to select the Radiello [143].

Regional observational networks have also been established for shorter periods of time. At select sites in the Southeastern Aerosol Research and Characterization (SEARCH) network [72], a more highly resolved approach has produced continuous 5-min observations of NH_3 since 2007 [150]. The NH_3 concentration is calculated based on the difference between the amount of oxidized nitrogen species produced through $>$ 95 % oxidation of flow through one denuder that does not collect NH_3 and another that does strip it from the air [150]. At a site collocated with an Interagency Monitoring of Protected Visual Environments (IMPROVE) site near Rocky Mountain National Park, two chemiluminescence monitors were deployed side by side to provide the reactive nitrogen gas concentration

Table 2 Summary of instruments measuring NH_3 that have been evaluated and deployed in North America

Instrument	Manufacturer	Deployment	Temporal resolution	Precision (uncertainty)	Detection limit	Citation
Phosphoric acid-based passive sampler	Radiello	AMoN	2 weeks	10 % (±40 %)	0.16 $\mu g\ m^{-3}$	Puchalski et al. [143]
Mini-parallel plate denuders	Met One	CSN (3 sites)	1 week	13 % (±40 %)	0.004 $\mu g\ m^{-3}$	Puchalski et al. [144]
Filter/denuder system	URG	Boulder, WY	~3.5 days	5.4 %(NR)	0.012 $\mu g\ m^{-3}$	Li et al. [100]
Polypropylene filters w/ phosphoric acid	SKC, Inc.	IMPROVE (select)	24 h	< 5 %[a] (±10 %)	0.018 $\mu g\ m^{-3}$	Chen et al. [29]
Denuder difference w/ chemiluminescence	URG, Thermo Scientific	SEARCH	5 m	NR (±15–20 %)[b]	250 ppt	Saylor et al. [150]
Instrument	Group	Range (ppbv)	Temporal resolution	Precision (uncertainty)	Detection limit	Citation
QC-TILDAS	Aerodyne Research, Inc.	30–1000	5 m avg[c]	14 pptv (NR)	42 ppt with 5 m avg	Ellis et al. [45]
CIMS (ground-based)	NOAA	0–3.5	10 s avg[d]	NR (±30 %)	100 pptv	Fehsenfeld et al. [53]
CIMS (aircraft-based)	NOAA	<0.07–80	1 s	NR (25 % ± 0.07 ppbv)	70 pptv	Nowak et al. [123]
Open-path QC laser	Zondlo (Princeton)	0.20–>2000	0.1 s	0.15 ppbv (0.20 ppbv ± 10 %)	300 pptv at 10 Hz	Miller et al. [111]

[a] Based on correlation coefficient between collocated measurements being 0.97

[b] Bias adjustment performed regularly against citric acid denuders

[c] 1-s resolution of measurement; averaged for optimal signal

[d] 4-s resolution of measurement; averaged for reliable signal

by difference for 1 year during the Rocky Mountain Atmospheric Nitrogen and Sulfur study [108]. Building upon this effort, a prototype of accurate and precise filter-based measurements of NH_x ($NH_3 + NH_4 = NH_x$) were added to select western USA IMPROVE sites from April 2011 to August 2012 [29]. This project demonstrated the potential for cost-effective monitoring of NH_x across the entire IMPROVE network and provided insight into seasonal NH_3 trends and influences [29]. The University Research Glassware (URG) denuder/filter system (URG, Inc., Model 3000CA) has often been deployed at specific locations as a benchmark for new techniques or for longer term measurements such as those taken in Boulder, Wyoming, during 2007–2011 [100]. These longer term measurements in single locations typically provide measurements integrated over multiple days or weeks and characterizations of larger trends.

Techniques to measure NH_3 with much higher temporal resolution have been developed more recently and deployed primarily in field campaigns. One such instrument is the chemical ionization mass spectrometer (CIMS) [52, 80]; two novel designs were deployed in the Aerosol Nucleation and Real-Time Characterization Experiment (ANARChE) campaign in 2002 [121]. Subsequently, an instrument was developed that was suitable for use in aircraft because of higher temporal resolution (approximately 5 s) and precision (100 ppt) needed for low NH_3 concentrations observed aloft [122]. With improvements in the inlet configuration and more effective purging of the instrument between flights, the CIMS has been employed in additional field campaigns including TexAQS [123] and CalNex [124] with 1-s time resolution. Another method of ascertaining NH_3 concentrations is the Aerodyne Research, Inc. Quantum Cascade Tunable Infrared Laser Differential Absorption Spectrometer (QC-TILDAS), which correlated well with a chemiluminescence-based measurement at 1-min resolution during an intercomparison campaign [45]. This closed-path instrument infers the ambient concentration from the absorption spectrum at 967 cm^{-1}, and it was deployed in the Border Air Quality and Meteorology study (BAQS-Met) [46]. The logistical limitations of these approaches, including power consumption and size, led to the innovation of a compact, open-path, high-sensitivity, QC laser-based atmospheric NH_3 sensor, which isolates the absorption signal of NH_3 at 9.062 μm [111]. To achieve a minimum detection limit of 0.30 ppbv at 10-Hz resolution, absorption at multiple points in the spectrum is isolated with multi-harmonic wavelength spectroscopy [111]. Online calibration reduces the effect of sensor drift, and the open-path design eliminates the measurement artifacts and time lag introduced by the inlet [111]. The dynamic range of the instrument is evident in the on-road observations collected with the instrument mounted atop a passenger vehicle in California and New Jersey in 2012 [166]. Together, these instruments have provided measurements of ambient atmospheric ammonia at the surface and aloft during field campaigns at higher temporal resolution than available through long-term monitoring networks. For comparison, a wide array of in situ NH_3 measurement techniques has been undertaken in other parts of the world. For example, simultaneous measurements were conducted of three different approaches in summer 2006 in Switzerland [120] and eleven in summer 2008 in Scotland [177]. Both of these studies highlighted the importance of careful inlet design, and the latter emphasized the robust agreement of the techniques at concentrations greater than 10 ppbv but discrepancies at lower concentrations.

Remote Sensing

While there have been tremendous strides in the availability of in situ measurements as described above, still the spatiotemporal coverage of such measurements is limited on continental to global scales. In contrast, remote sensing measurements of NH_3 provide a new means of broadening our understanding of the sources and distribution of reactive nitrogen, especially over regions where there are little or no observations and the emission sources are poorly known. To date, there are lower tropospheric NH_3 retrievals from several infrared instruments in sun-synchronous low-earth orbits (LEO), and their attributes are summarized in Table 3.

The NASA Tropospheric Emissions Spectrometer (TES) [14] Fourier Transform Spectrometer (FTS) was launched on the Aura satellite on July 15, 2004. TES has a high spectral resolution of 0.1 cm^{-1} (apodized), good radiometric noise of $\sim 0.1 - 0.2$ K at 280 K [156, 185], is in an orbit that includes a mid-day overpass ($\sim$1:30 a.m. and 1:30 p.m. LST), and has a relatively small spatial footprint of 5×8 km^2 , all of which are favorable conditions for boundary layer NH_3 detection. One limitation of the TES global survey NH_3 observations is the lack of spatial density, as the spacing between consecutive observations can be as large as 180 km, with a repeat cycle of 16 days. TES provided the first detection of boundary layer NH_3 from space [15], but since then, there have been a number of space-based lower tropospheric NH_3 observations that have contributed to improving our understanding of atmospheric NH_3. The Infrared Atmospheric Sounder Interferometer (IASI) [33] FTS launched on two MetOp satellites has also provided very valuable NH_3 observations [67, 76, 86, 147, 169, 172]. IASI is a scanning sensor that provides broad spatial coverage approximately 3 h earlier than TES. The spectral resolution of IASI is coarser than TES while the spectral radiometric noise in the NH_3 retrieval regions is similar (see Table 3). Both TES and IASI have measured temporal and spatial distributions of lower tropospheric NH_3 concentration values regionally (e.g., [15, 32]) and globally [31, 157,

Table 3 Overview of current and potential NH_3 remote sensing capabilities

Instrument	Across track scanning	Launch date	Resolution[a] (cm^{-1})	Noise[b] level (K)	~Overpass time (local)	Footprint area or diameter
TES	No	07/15/2004	0.10 (0.06 unapodized)	0.1–0.2	1:30 a.m., p.m.	8×5 km^2
IASI (MetOp-A)	Yes	10/19/2006	0.5	0.15–0.2	9:30 a.m., p.m.	12 km
IASI (MetOp-B)	Yes	09/17/2012	0.5	0.15–0.2	9:30 a.m., p.m.	12 km
CrIS	Yes	10/28/2011	0.625	0.04	1:30 a.m., p.m.	14 km
AIRS	Yes	05/04/2002	0.8	0.2	1:30 a.m., p.m.	13.5 km
GCIRI	Yes	–	0.10 (0.06 unapodized)	0.1–0.2	Hourly	4×4 km^2

[a]In the 967 cm^{-1} NH_3 spectral band

[b]At 280 K

172] and thus far have provided the bulk of the available satellite NH_3 observations for air quality purposes.

However, there are new observations from the Cross-track Infrared Sounder (CrIS) FTS instrument on board the NOAA/NASA/DoD Suomi National Polar-orbiting Partnership (NPP) satellite launched in 2011 that have demonstrated to also provide lower tropospheric NH_3 observations [155]. Many of the CrIS instrument characteristics are very similar to IASI (see Table 3), but it has four times lower noise than TES and IASI, and the early afternoon daytime overpass time, allowing it to approach the retrieval capabilities of the higher spectral resolution TES observations. There are also potential NH_3 observations (Warner et al. 2014) from the Atmospheric Infrared Sounder (AIRS) grating spectrometer [8] launched on the LEO NASA Aqua satellite in 2002 with similar overpass times to TES and CrIS. AIRS also has the broad spatial coverage of a scanning instrument (similar to IASI and CrIS, see Table 3) but with a slightly reduced spectral resolution and similar radiometric noise [170].

Satellite observations of NH_3 are inferred from measured spectral radiances, which generally requires a complex retrieval inversion process with assumptions on the profile shape and variability (e.g., [32, 155, 157, 172]). Since the infrared NH_3 signal is relatively small (<1 K brightness temperature) compared to the overall background signal (order of 300 K brightness temperature), there is limited information that can be obtained from satellite retrievals. TES has the most sensitivity to NH_3 concentrations on a per retrieval basis. Shephard et al. [157] showed that the TES NH_3 retrievals: (i) have a minimum detection level corresponding to a profile with a surface volume mixing ratio of ~1 ppbv, (ii) typically have peak vertical sensitivity in the boundary layer between 900 and 700 hPa (1–3 km), and (iii) provide ~1 piece of information (degrees-of-freedom-for-signal, DOFS) under favorable retrieval conditions. While TES recovers a vertically resolved NH_3 profile, we often consider the averaging kernel weighted mean of this profile, aka the Representative Volume Mixing Ratio or RVMR. This single concentration estimate has less dependence on the algorithm's a priori profile and is more easily visualized in 2D. A full description of the RVMR and the determination of measurement limits is provided in Shephard et al. [157]. Typical measured RVMR values directly over NH_3 source regions in North America are above 10 ppbv; mean values over the entire central USA are ~1.5 ppbv [157].

Since these satellite retrievals can be challenging, it is important to evaluate the satellite measurements with other available observations. Given the sampling differences between satellite and in situ observations, and the fact that NH_3 is very inhomogeneous over small distances, performing direct validations of the lower tropospheric satellite observations with sparsely available (mostly at the surface) in situ NH_3 observations is difficult. There have been some very valuable indirect correlation comparisons performed to demonstrate the quality of the satellite NH_3 observations. It has been shown that the TES NH_3 observations are well correlated with the in situ observations both spatially and seasonally [136]. Similarly, IASI NH_3 total column retrievals compare well with indirect in situ surface and aircraft measurements [173]. Total column values estimated from simultaneous aircraft and surface measurements during the DISCOVER-AQ campaign in California in 2013 [166] are within the estimated uncertainty of the TES total column measurements. Initial CrIS comparisons during the same campaign show that it qualitatively captures the spatial variability of the boundary layer NH_3 concentrations as revealed by nearby in situ surface observations and TES satellite observations; the quantitative differences between the CrIS and TES boundary layer observations are often within the estimated retrieval uncertainty of the two measurements [155]. During a recent intensive Joint Canada-Alberta Oil Sands Monitoring (JOSM) field campaign, TES

and aircraft NH_3 direct volume mixing ratio profile comparisons were carried out, where the assumed prior information (i.e., profile shape) and broad vertical resolution of the satellite retrievals have been taken into account [154]. From these direct comparisons under conditions where the NH_3 volume mixing ratio amounts were relatively small (median value of 1.0 ppbv at 900 hPa), the actual errors show a small bias of ~+7 % with a standard deviation of ~±25 % at 825 hPa height, which is consistent with the estimated TES NH_3 retrieval bias of +7 % based on simulations [157] and the TES reported estimated retrieval uncertainty of ~±30 %.

These new LEO satellite remote sensing observations have already proven useful for evaluating model estimates of NH_3 distributions and inverse modeling of NH_3 sources in both regional and global chemistry transport models. Both TES and IASI observations have revealed broad underprediction of NH_3 concentrations in the models. For example, Shephard et al. [157] showed using TES data that the global GEOS-Chem model (in which NH_3 emissions for anthropogenic and natural sources were based on the 1990 GEIA inventory [21] with monthly variation scaled according to Gilliland et al. [65]) under-predicted NH_3 concentrations over most of the globe, with a bias of monthly mean RVMR over 4 years (2006–2009) larger than 7 ppbv in Asia. Walker et al. [179] (using TES) and Heald et al. [76] (using IASI) showed underestimation of NH_3 over California in GEOS-Chem (based on the EPA NEI 2005) by −79 % (normalized mean bias) of RVMR and more than 0.3×10^{16} molec cm^{-2} of the vertical column concentration, respectively, leading to a local underestimation of ammonium nitrate aerosol. Similarly, Kharol et al. [86] when investigating the sensitivity of inorganic aerosol to NO_x emissions showed that GEOS-Chem generally under-predicted NH_3 observations over Asia (using NH_3 emissions from Streets et al. [165] with a 30 % reduction) compared with IASI NH_3 observations by more than 0.5×10^{16} molec cm^{-2}. Zhu et al. [190] used TES NH_3 observations to provide top-down (inverse modeling) constraints on NH_3 emissions in GEOS-Chem, which improved the normalized mean bias between model and AMoN observations by up to 90 %. Also, coincident TES observations of NH_3 and CO have been used to demonstrate the potential of using remote sensing data to identify NH_3 emission sources and constrain emission inventories (e.g., [107]). TES observations in combination with surface and aircraft NH_3 observations have also been used to provide insight on the treatment of the diurnal variability of NH_3 from livestock emissions and bidirectional fluxes in both GEOS-Chem and the regional Community Multiscale Air Quality (CMAQ) model (e.g., [191]).

NH_3 Measurement and Modeling Frontiers

Improved Mechanistic Models of NH_3 Sources and Sinks

Estimation of the global anthropogenic influence on the nitrogen cascade through NH_3 production and use was first quantified with the Moguntia Eulerian tropospheric model [42]. Higher resolution estimates of NH_3 emissions followed [21], and these inventories continue to be refined through top-down and bottom-up analysis (e.g., [130, 134]). Additionally, representations of inorganic aerosol thermodynamics, which capture the volatility of NH_3 from suspended aerosol, were developed in tandem with these three-dimensional models (e.g., [11, 87, 88, 119]). Furthermore, the interactions of NH_3 with ecosystems were determined to be a function of a canopy compensation point, which reflects the bidirectional exchange of NH_3 [6]. As described below, not until recently have modeling approaches that quantify these fluxes been implemented in three-dimensional chemical transport models [56]. Integration of this model and emission inventory developments into regional (e.g., CMAQ [10]) and global chemical transport models (e.g., GEOS-Chem [191]) will enable the environmental decision-making community and scientists to better understand the dynamic interplay between NH_3 emissions, deposition, and climate [169].

The dry deposition scheme in most air quality models is based on the resistance in series formulation of Wesely [182], which only considers the unidirectional flux of NH_3 from the air to the surface. However, the air-surface exchange is known to actually be bidirectional, e.g., the net flux can either be evasion or deposition [56]. Two different strategies have been used in regional and global air quality models to capture the bidirectional nature of NH_3 air-surface exchange: (i) Models that have parameterized the flux based on empirical relationships [91] or lookup tables for different land use types [39]. (ii) Semi-empirical process-based models that parameterize agricultural nitrogen management, the soil NH_4^+ pool, and model the flux between the atmospheric and soil pools [10, 59, 191]. In the second type of model, the total air-surface exchange flux is calculated as a function of the gradient between the ambient NH_3 concentration in the first (surface) layer of the model and the canopy compensation point [10, 139](see Fig. 1). The latter is calculated as a function of temperature and NH_3 emission potential, which in turn depends upon the concentrations of NH_4^+ in the soil pool. More details of this bidirectional scheme can be found in Cooter et al. [34], Cooter et al. [35], and Pleim et al. [139]. The overall impact of the NH_3 bidirectional exchange process is to effectively

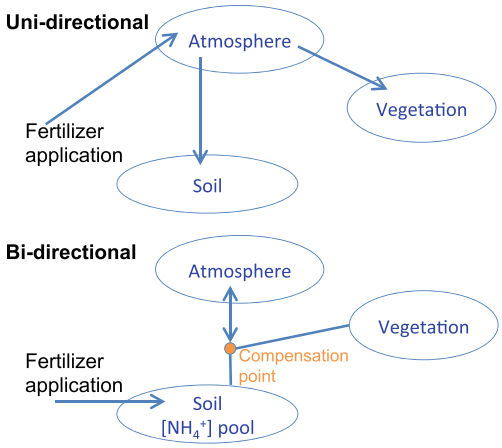

Fig. 1 Schematic of unidirectional versus bidirectional treatment of NH_3 deposition and emission

enhance the atmospheric lifetime of NH_3 through the regulation of deposition, and the storage of deposited NH_3 in a soil pool where it can later re-emit.

Both CMAQ and GEOS-Chem have recently been updated to included representation of NH_3 bidirectional exchange, as well as improved diurnal variability of NH_3 from livestock. While the detailed equations governing these mechanisms are provided in these papers, here we qualitatively describe these features. The standard, static, NH_3 livestock emissions in models such as GEOS-Chem are evenly distributed throughout the 24 h of each day of the month. That the simulated NH_3 livestock emissions did not have significant diurnal variation is a likely explanation for large ($\sim\times 2$) nighttime overestimates of NH_3 of both of these models with hourly ammonia observations. European models use empirical relationships with wind speed and temperature to derive a diurnal profile [161] for livestock emissions. Here, we describe a more physically based empirical diurnal profile for the hourly NH_3 livestock emissions similar to the work done for sea bird colonies by Riddick et al. [148]. Here, we assume that animal NH_3 emissions originates from ammonium in the manure solution and is transported from the emission sources via atmospheric processes. The diurnal profile was applied to monthly emissions (1) to preserve the different animal emission factors and seasonality introduced in the compilation of emissions,

$$E_{NH_3}(t) = \frac{c_T(t)/R_{ATM}(t)}{\overline{c_T}/\overline{R_{ATM}}}\overline{E_{NH_3}}, \quad (1)$$

where, E_{NH_3} is the ammonia emissions, c_T is the combined Henry and dissociation equilibria for NH_3 and NH_4^+ following Nemitz et al. [118], R_{ATM} is the atmospheric resistance, and t is time. The overbars indicate monthly averages. The results from Eq. 1 estimated much lower nighttime emissions and higher rates of emissions during the daytime (Fig. 2). Hourly emissions are calculated from monthly emissions using hourly changes to the aerodynamic resistance and Henry's equilibrium coefficient as function of surface temperature. This new diurnal distribution scheme (referred to later as the dynamic scheme) for NH_3 livestock emissions has been developed in CMAQ and implemented in GEOS-Chem. The overall impact of this scheme, in both models, is to decrease livestock NH_3 emissions at night, when temperatures are colder, and to increase them during the day. We recognize, however, that this treatment is only an initial step given that livestock in different regions are subject to different husbandry practices.

The Value of Geostationary Remote Sensing Measurements for NH_3

IASI and CrIS are both integral to operational meteorological polar-orbiting systems. IASI has already been launched on two MetOp satellites, and there are plans for at least one more launch. CrIS is expected to be deployed on future NASA/NOAA Joint Polar Satellite System (JPSS) satellites. Both sensors will thus continue to provide global NH_3 observations for many years. Although these current LEO polar-orbiting space-based sensors are yielding unprecedented NH_3 observations in the lower troposphere and boundary layer globally, the restricted diurnal sampling and large footprint size of the observations limits the characterization of some of the fundamental aspects of the NH_3 emissions, especially the issues identified in the previous section: the dependence of NH_3 bidirectional exchange on the surface emissions potential, and the diurnal variability of NH_3 emissions from livestock operations.

The GEO-CAPE mission [55], recommended in the NASA decadal survey [125], would provide geostationary measurements of tropospheric constituents relevant to air quality and climate for the first time over North America. The high spatial and temporal resolution of GEO-CAPE (hourly observations every ~4 km) offers new possibilities for constraining emissions that are not achievable with low-earth-orbit (LEO) platforms, such as allowing nearby pollution sources to be separated and observed individually, e.g., roads, farms, or point sources in densely populated regions. Geostationary observations would also provide critical tests for the temporal behavior of existing inventories and could improve mechanistic models that predict emissions when direct observations are not available. As part

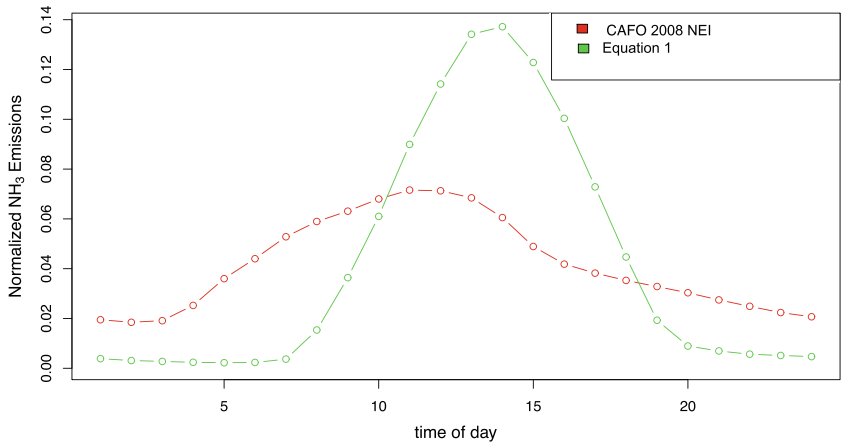

Fig. 2 July, 2007, CMAQ continental US hourly emissions fraction (dimensionless) using the static profile (*red*) and the dynamic profile (*green*). Note that the static profile is the same for each day, whereas the dynamic profile varies with atmospheric conditions

of GEO-CAPE, the Tropospheric Emissions: Monitoring of POllution (TEMPO) mission is slated for launch in 2019. This instrument will measure in the UV and visible range, making hourly observations at 4-km resolution primarily of NO_2 and ozone. With this spectral range, TEMPO will not measure the absorption of species such as CO, CH_4, or NH_3. For these species, the GEO-CAPE science team supports a second mission, named GCIRI (GEO-CAPE InfraRed Instrument), which would complement TEMPO with measurements in the IR range necessary to detect these species.

Here, we explore the potential of a GCIRI geostationary measurement of NH_3 to fundamentally improve our understanding of NH_3 sources at a mechanistic level, focusing on the diurnal variability and bidirectional flux of NH_3 as described in Section "Improved Mechanistic Models of NH_3 Sources and Sinks." This will allow for enhancements to air quality models that outlast the lifetime of the instrument itself (a uniquely different goal from, e.g., forecasting or monitoring). We thus consider two case studies that address the following questions: (1) Would GCIRI observations be able to evaluate uncertainties in fertilizer application rates and bidirectional NH_3 fluxes? (2) Would GCIRI observations allow for improved representation of the diurnal variability of livestock emissions in air quality models? For both, we consider the information from both GCIRI and existing LEO instruments, and we evaluate the impacts of model adjustments on estimates of aerosol nitrate.

While real geostationary measurements NH_3 are not yet available for analysis, we can instead generate pseudo-observations from a geostationary instrument, GCIRI, as well as a LEO instrument, by sampling modeling values as if they were the real atmosphere, and applying satellite retrieval algorithms to these samples. For the GCIRI instrument specifications in this Observing System Simulation Experiment (OSSE), we have been fairly conservative and adopted the instrument spectral resolution and measurement noise from the TES instrument, see Table 3; its combination of spectral resolution and instrument noise provides the most accurate present day boundary layer (0–2 km) NH_3 sensitivity observed from space. This approach does though neglect uncertainties owing to model transport error. However, it should be noted that a future GCIRI-type instrument is likely to benefit from even lower instrument noise (more similar to CrIS instrument noise), with spectral resolution somewhere in the 0.1 cm^{-1} (TES) to ~0.5 cm^{-1} (IASI and CrIS) range. Furthermore, GCIRI's actual horizontal spatial footprint of 4 km at the center of the domain will provide better sampling of local emission sources (e.g., large cities, agricultural regions, and oil extraction areas) than what is represented in our 12-km scale OSSE.

Constraints on Bidirectional Exchange

Here, we consider a case study to evaluate how variations in NH_3 concentrations owing to the bidirectional exchange of NH_3 at the surface may or may not be discernible using space-based measurements. Modeled WRF and CMAQ 12×12 km^2 simulations were conducted for June of 2006 and include all anthropogenic emissions from the 2005 EPA National Emissions Inventory scaled to 2006 using 2006 continuous emissions monitoring observations and 2006 WRF modeled meteorology. These simulations are described in detail in Dennis et al. [40]. Results from CMAQ simulations with standard unidirectional NH_3 emissions are shown in the left panel of Fig. 3. The impacts of bidirectional exchange are evaluated by repeating this simulation, using the bidirectional NH_3 emissions scheme from Bash et al. [10], and the results are shown in the center panel. The shift in the patterns between the base and bidirectional case is due to the NEI estimation of fertilizer NH_3 emissions based on fertilizer sales within the county and a prescribed seasonal profile. In the bidirectional exchange case, fertilizer application is modeled based on modeled plant nutrient demand, fertilizer application method, and modeled soil biogeochemistry at the model

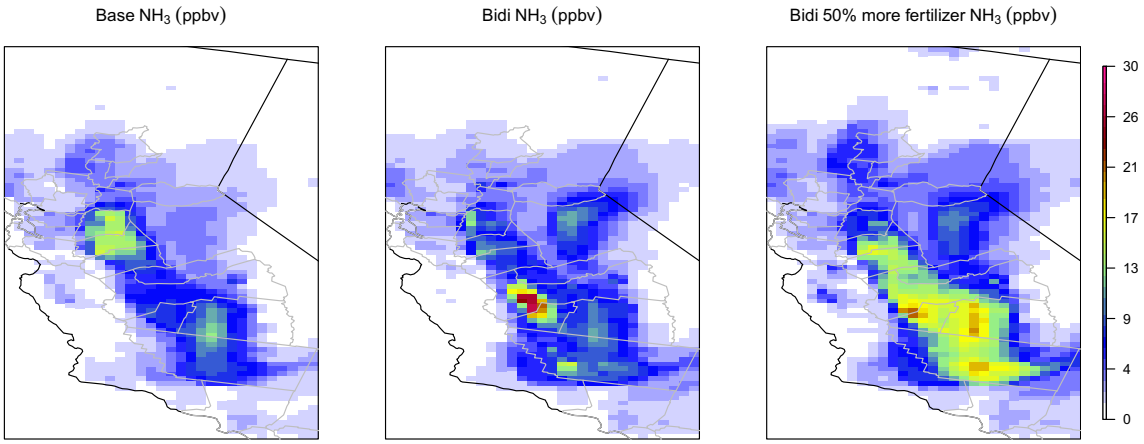

Fig. 3 Average surface-level NH_3 concentrations over southern California from CMAQ simulations using (*left*) unidirectional NH_3 emissions (*center*) bidirectional NH_3 fluxes, and (*right*) bidirectional NH_3 fluxes with enhanced fertilizer application rate

grid cell resolution [35]. Note that the simulations used here are a subset of the simulations in Dennis et al. [40]. In these simulations, the +50 % gamma case had a simple look up table for the mesophyll gamma while the bidirectional case used the mesophyll gamma parameterization from Massad et al. [110] resulting in higher mesophyll NH_3 compensation points for crops and thus the increase in ambient NH_3 seen in the center panel of Fig. 1. The model was found to be most sensitive to the fertilizer application and soil compensation point in agricultural areas [40]. One of the larger sources of uncertainties in implementing such a scheme is the fertilizer application rate. We thus also consider a third simulation, right panel, which shows surface-level NH_3 concentrations when the fertilizer rate is increased by 50 %.

We next use these CMAQ simulations to generate both LEO and GCIRI pseudo observations of NH_3 RVMR. The maps in Fig. 4 show differences in GCIRI pseudo observations between these scenarios. The red X's indicate locations where LEO measurements from TES were available from a standard global survey retrieval. Their values would be the same as those from GCIRI, just limited to these locations. The maps show the difference between cases with the standard unidirectional NH_3 emissions (Base), bidirectional exchange (Bidi), and bidirectional exchange with enhanced fertilizer application (Fert). The maps obtainable from a GCIRI type measurement clearly show key differences between the Base and Bidi simulations, with the latter leading to smaller RVMRs in the western part of the domain and larger values in the Central Valley (the region with concentrations above 10 ppbv in Fig. 3).

LEO transects from TES, on the other hand, would not have been capable of making these distinctions given their sparse sampling—the differences in RVMR across scenarios at the LEO transect locations are rarely larger than 0.4 ppbv, which is close to the retrieval uncertainty of ±30 % (although the differences are >5 ppbv elsewhere). Measurements from CrIS have similar levels of uncertainty, but a much more complete spatial coverage (see Section "Remote Sensing"), with a spatial resolution similar to that of the 12 × 12 km^2 model resolution used in these tests. Assuming that CrIS measurements are normally distributed with an uncertainty of ±30 %, we consider the differences shown in the left, center, and right panels of Fig. 4 and calculate that the percentages of the grid cells for which these differences are statistically significant (p value <0.1) to be 18, 37, and 17 %, respectively. Given that GCIRI would have ∼7 times the sampling density of CrIS, we assume a ±10 % error at the 12 × 12 km^2 scale

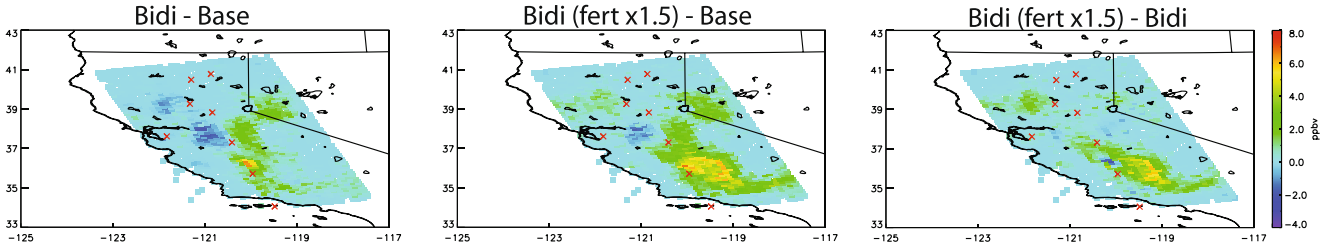

Fig. 4 Differences in GCIRI RVMR values corresponding to three different atmospheres from the CMAQ simulations showing in Fig. 3: Base (unidirectional NH_3 emissions), Bidi (bidirectional fluxes of NH_3), and Fert (bidirectional fluxes of NH_3 with a 50 % increase in fertilizer). Also shown (*red* X's) are the locations during this time period where there were LEO observations available from TES

and evaluate the ability of GCIRI to discriminate between these simulations. With GCIRI, differences across the left, center, and right panels are visible 43, 70, and 46 % of the time, respectively. While we have not yet performed any top-down inverse modeling studies with such datasets, these results suggest that GCIRI would be able to distinguish between fundamentally different drivers of NH_3 sources much more often than existing LEO measurements. This provides qualitative evidence that GCIRI would provide new information for improving model treatment of NH_3 emissions at a process level. We do note that the differences between the models tested here are admittedly quite stark, hopefully more-so than model uncertainty by a potential 2020 launch, and we have assumed clear-sky conditions which will overestimate the spatial sampling benefits of GCIRI. However, here we have also only considered measurements once-per-day; the additional benefit of hourly measurements for GCIRI are explored in the next case study.

We also evaluate the differences in these scenarios in terms of impact on NO_3^- aerosol. Figure 5 shows measured and modeled surface-level aerosol NO_3^- at CSN (top) and IMPROVE (bottom) sites. Nitrate generally increased in the Central Valley of California in the summer when using the bidirectional exchange scheme due to an increase in the NH_3 concentrations largely from a reduction in the NH_3 dry deposition and abundant NO_x. Note that this is specific to this domain at during this time and that nitrate aerosol reductions have been observed in other parts of the country during the spring and fall due to the implementation of

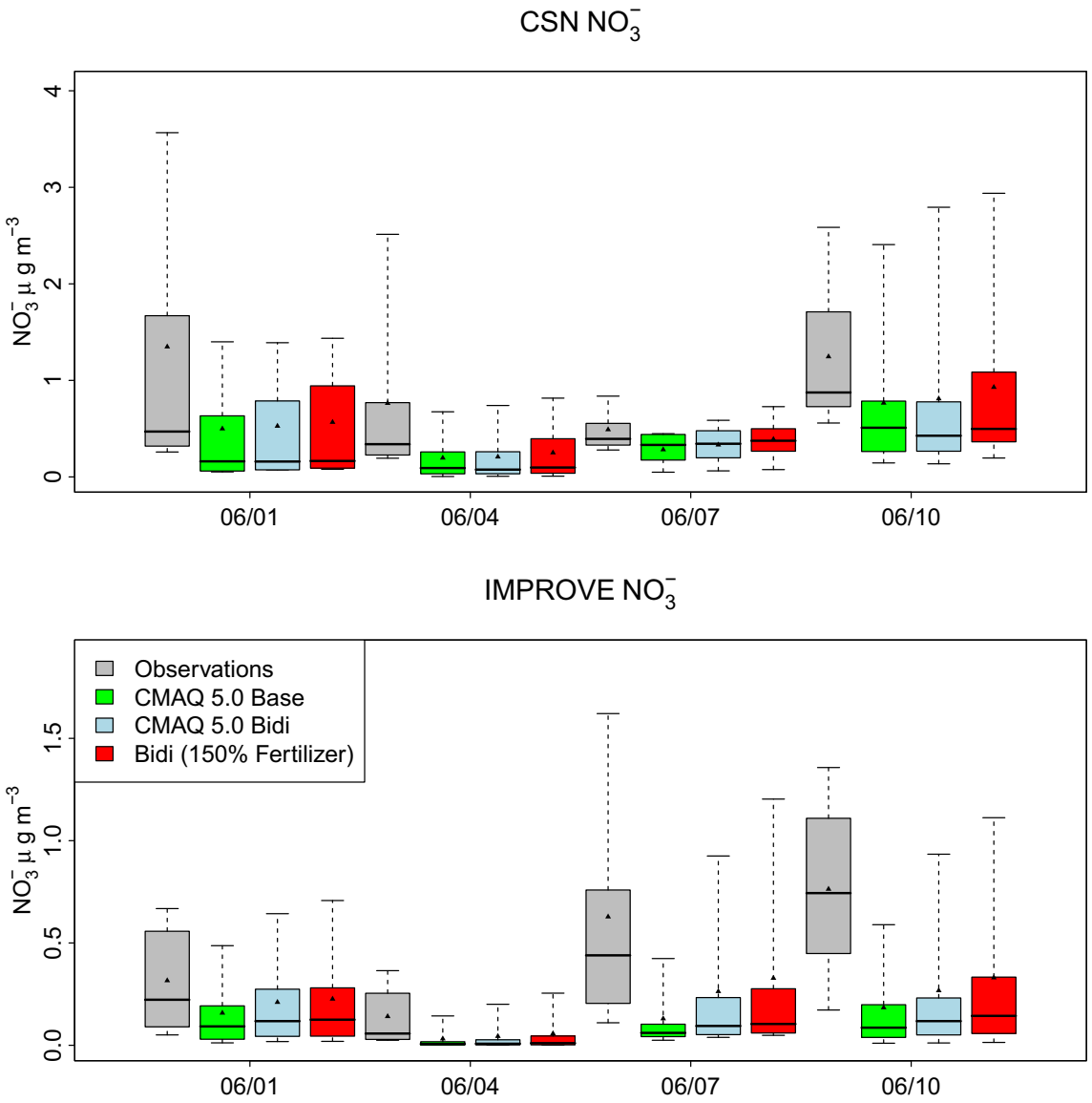

Fig. 5 CMAQ model estimated surface-level nitrate aerosol concentrations in CA compared to observations of (*top*) CSN and (*bottom*) IMPROVE. Simulations include the Base case (unidirectional NH_3 emissions), the Bidi case (bidirectional exchange of NH_3) and a bidirectional simulation with 50 % higher fertilizer application rates

the bidirectional exchange option in CMAQ [10]. CMAQ hourly NO_3^- aerosol estimates were paired in time, averaged to the 24-h sampling frequency, and space with the 9 CSN sites and 11 IMROVE sites in the modeling domain. Total $PM_{2.5}$ exceeded 20 μg m^{-3} at CSN sites during this time period, more than 10 % of which was NO_3^-. First, we note that the implementation of NH_3 bidirectional exchange causes NO_3^- to increase relative to the base case simulation at all times and locations—by 10 % at the CSN sites and 44 % at the IMPROVE sites. This occurs even though NH_3 levels are typically quite high in the Central Valley, and nitrate formation is thought to be limited more by NO_x than NH_3. Increasing the fertilizer emissions by 50 % results in additional increases of NO_3^- at CSN sites by 21 % and IMPROVE sites by 19 %. In comparison to the observations, we also note that the base case version of the CMAQ model has a low-bias with regards to nitrate observations in California at this time of year. This bias is reduced by 10 % at CSN sites and by 20 % at the IMPROVE sites in the Bidi case, with even further improvements if fertilizer is increased. However, the remaining biases in nitrate in California may be related to model biases in other particulate bases or missing processes [85]. This case study indicates that such model improvements, which are potentially constrainable by GCIRI observations, could have measurable and meaningful impact on estimates of aerosol, in addition to further understanding the factors that control $PM_{2.5}$ concentrations.

Constraints on Diurnal Variability

The second question we address is whether or not GCIRI observations could provide constraints on the diurnal variability of NH_3 emissions from livestock. It is known that

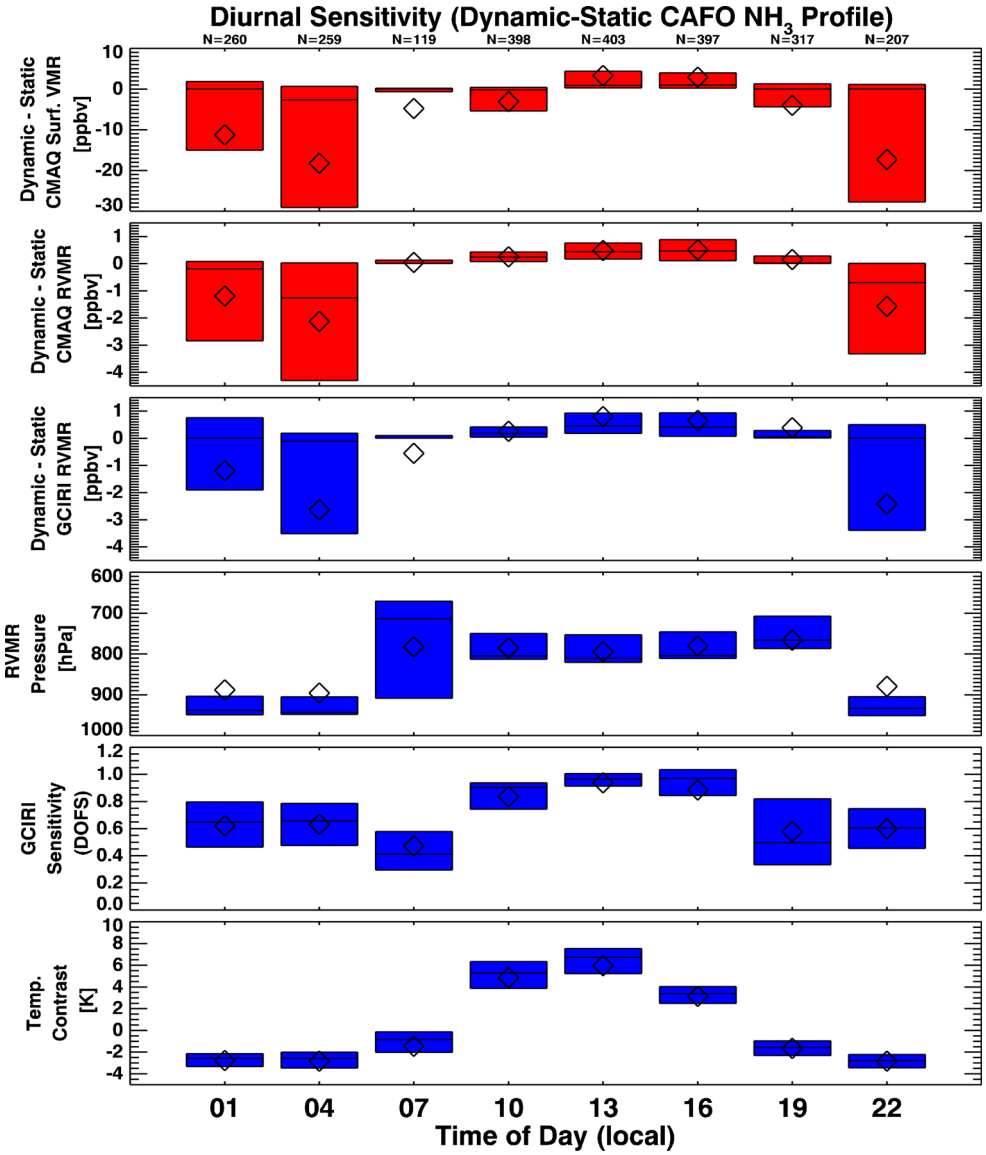

Fig. 6 Results of CMAQ model simulations using dynamic-static diurnal emissions reported as a function of local time of day. The *top panel* shows differences in the model surface concentrations between runs with dynamic and static diurnal Concentrated Animal Feeding Operations (CAFO) emissions. The *second panel* shows the same differences as the top panel, but for the model computed RVMR values, which can be compared to the corresponding pseudo geostationary satellite (GCIRI) RVMR observations shown in the *third panel*. The *fourth panel* show the pressure levels of the RVMR values used in the second and third panels. The pseudo satellite retrieved GCIRI sensitivities reported in terms of degrees-of-freedom for signal (DOFS) are plotted in the fifth panel. The *bottom panel* contains the atmospheric thermal contrast between the surface and the first profile level. The box edges are the 25th and 75th percentile, the line in the box is the median, and the diamond is the mean

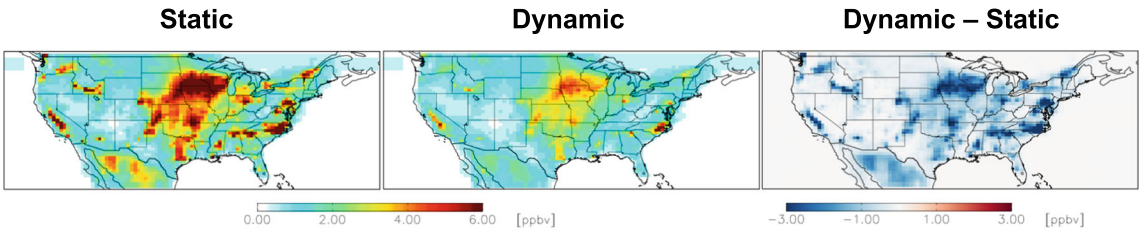

Fig. 7 Average surface-level NH_3 over the USA during July, 2006, from GEOS-Chem high-resolution (0.5° × 0.667°) simulations. Static simulations contain invariant diurnal NH_3 livestock emissions

the diurnal variability of NH_3 sources strongly affects surface-level concentrations nearby. What has not been shown is whether or not the impact of this variability is significant enough to cause detectable changes in the NH_3 vertical profile seen by satellites, i.e., changes occurring at altitudes in the 900–700 hPa range.

Here, we consider results from experiments performed using simulations from the CMAQ model run at the 12×12 km^2 scale using the same statics versus dynamic emissions schemes described in Section "Improved Mechanistic Models of NH_3 Sources and Sinks." Only days in which at least four time periods have retrievals with DOFS >0.4 are selected in the analysis. Plus, only the individual results in which there were at least 0.1 DOFS were considered to ensure that there was some information being provided by each observation. These are shown in Fig. 6, where results plotted in red indicate the simulated atmospheric conditions and results in blue show the conditions as detected by GCIRI. The top panel shows the difference between the CMAQ model surface concentrations from the dynamic case minus the static case in locations in California with dominant livestock emissions on July 22, 2006. In the second row of Fig. 6, the differences in CMAQ RVMR values are shown, and in the third row, the differences in RVMRs detectable from the GCIRI instrument are shown. The latter demonstrates that the GCIRI instrument is indeed able to detect significantly lower NH_3 concentrations at night, with a mean difference of −2.6 ppbv at 4 a.m. and slight increases during the day, with a mean difference of up to 0.7 ppbv in the mid-afternoon (1–4 p.m.). These parameters highlight the reduced retrieval sensitivity and range of peak pressure sensitivity levels at 7 a.m., resulting in less valid comparisons at this time of the day. Also shown in this figure is the pressure level of the peak instrument sensitivity that contributes to the RVMR, the DOFS, and the temperature contrast. Despite the smaller temperature contrast at night, the differences in NH_3 concentrations between the static and dynamic cases are still detectable. This OSSE demonstrates that a GCIRI-type geostationary would generally be able to capture the expected difference between different diurnal NH_3 emission profiles, and it would be a valuable tool in advancing our understanding of NH_3 emissions in North America.

Supposing that the dynamic emissions of NH_3 from livestock are eventually an observable feature of air quality models, it is of interest to evaluate the impacts of such an enhancement to NH_3 simulations more broadly. We thus consider the impact of the diurnal variability of livestock NH_3 emissions over the USA. The dynamic scheme for NH_3 livestock emissions described in Section "Improved Mechanistic Models of NH_3 Sources and Sinks" is implemented in 0.5° × 0.667° resolution GEOS-Chem simulations for July 2006. We also perform simulations using the standard livestock emissions (constant monthly values), aka the static case. Plots of the spatial distribution over the USA in July of 2006 of NH_3, nitrate, and nitrogen deposition, are shown in Figs. 7, 8, and 9. The impacts of livestock emissions' diurnal variability on monthly mean NH_3 concentrations can be significant, up to 50 %. Concentrations are reduced as less NH_3 is emitted into shallow boundary layers during the night using the dynamic scheme; instead, emissions peak during the day, when dynamic export away from the surface is more efficient and the increased boundary layer height (relative to nighttime) decreases the NH_3 concentration. There are corresponding reductions in aerosol nitrate. For both NH_3 and nitrate, some of the largest decreases are in spatially isolated regions, such as the San Joaquin Valley

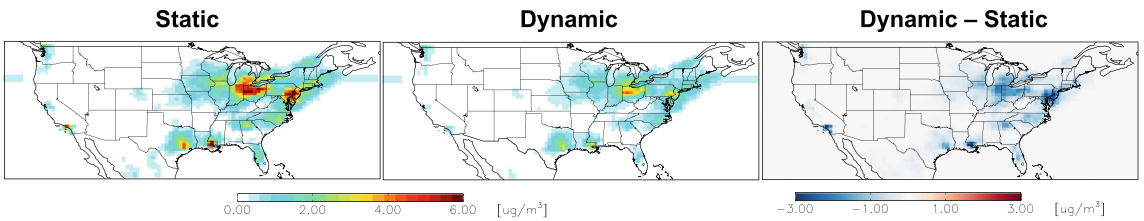

Fig. 8 Average surface particulate nitrate over the USA during July, 2006, from GEOS-Chem high-resolution (0.5° × 0.667°) simulations. Static simulations contain invariant diurnal NH_3 livestock emissions

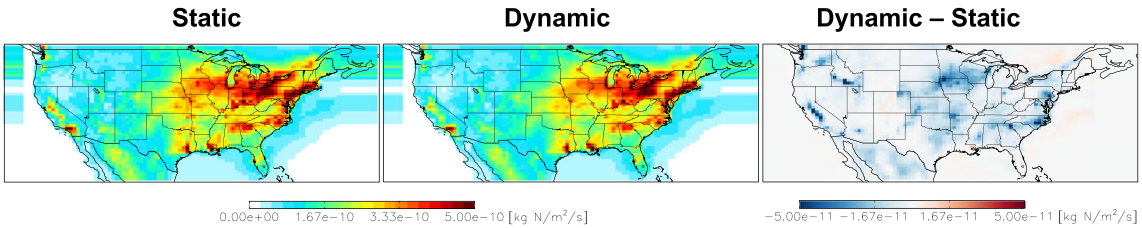

Fig. 9 Total nitrogen deposition in the USA during July, 2006, from GEOS-Chem high-resolution (0.5° × 0.667°) simulations. Static simulations contain invariant diurnal NH_3 livestock emissions

for NH_3, or the New Jersey area for nitrate. These changes are much weaker in the global 2° × 2.5° simulations of Zhu et al. [191]; thus, it seems likely that the impacts of the dynamic diurnal variability scheme may be particularly important for higher-resolution nested models. Regardless, the impacts on nitrogen deposition however are fairly small, impacting total reactive nitrogen less than 10 %, as oxidized nitrogen dominates reactive nitrogen deposition in much of the country (e.g., [47]).

Conclusions

In this review, we have considered recent progress in observing, modeling, and quantifying the impact of NH_3 on many aspects of our environment. Recent research has highlighted the outsized role that NH_3 plays in air quality, climate, and deposition of reactive nitrogen owing to several factors: (i) NH_3 concentrations have risen considerably since pre-industrial times and are projected to continue to rise globally, (ii) particulate matter concentrations are often highly sensitivity to NH_3 levels that dictate ammonium nitrate formation, (iii) declines in SO_2 emissions will exacerbate the aforementioned effect, and (iv) formation of ammonium nitrate facilitates long-range transport of reactive nitrogen and its ultimate deposition in sensitive ecosystems and water bodies. Commensurate with these research developments are efforts to expand measurement and modeling capabilities for NH_3. New routine monitoring, precise in situ mobile measurements, and remote sensing platforms have helped transform our ability to evaluate NH_3. This in turn has spurred enhanced development of the representation of NH_3 in air quality models. Ultimately, we hope this cyclic process will provide a stronger basis for developing policy that takes advantage of the efficiency of NH_3 emissions controls in mitigating a wide-range of environmental concerns in North America.

In addition to considering the significant research strides made in recent years, we also look to the potential of future remote sensing measurements to help further our understanding of NH_3, particularly the interplay between emissions, deposition, and climate. Towards this end, we present new work assessing the value of GEO versus LEO remote sensing observations for constraining fundamental processes governing NH_3 and ammonium nitrate aerosol in air quality models: the diurnal variability of NH_3 emissions from livestock sources and bidirectional exchange of NH_3 from soils. In our first case study, we demonstrate that even though bidirectional exchange largely impacts surface-level NH_3, whereas thermal IR instruments are most sensitive to NH_3 levels 1–2 km above the surface, a theoretical geostationary IR instrument (GCIRI) would clearly detect differences in NH_3 distributions owing to the bidirectional fluxes of NH_3 from soils, in conditions where current LEO measurements would not. These differences, even in regions such as the Central Valley of California which are already NH_3 rich, are shown to have notable impacts on model estimated aerosol nitrate, reducing the model bias by 10–20 % relative to surface-level observations.

In our second case study, we found that over the USA, the differences between a constant monthly NH_3 emissions and one in which the livestock emissions respond dynamically to local environmental conditions on an hourly basis is not detectable in the national-scale average NH_3 profiles by LEO instruments (e.g., TES), even though such differences may impact surface-level aerosol nitrate by up to 50 %. Some small differences are currently detectable over select locations, such as when restricting analysis to a few grid boxes in California where the satellite retrieval DOFS were high (>0.5) and the local emissions were dominated by livestock sources (>75 %), yet, the differences were still less than a fraction of a parts per billion. In contrast, simulated geostationary observations generated from CMAQ simulations similarly show large (up to 2.5 ppbv) signals in the difference between day and nighttime concentrations.

These two case studies demonstrate the advantages of the spatiotemporal coverage of geostationary observations, even when instrument sensitivities peak above the surface level, for improving our understanding of the diurnal variability and bidirectional exchange of NH_3 sources. Likewise, validation of these geostationary observations with in situ observations/aircraft measurements will also be needed

in the future studies. As air quality models evolve to simulate these processes, the value of a geostationary instrument to constrain these processes over wide spatial and temporal scales is becoming increasingly important. The impacts of detailed NH_3 source modeling is shown here to have significant impacts on aerosol nitrate, and hence $PM_{2.5}$. Further studies may also evaluate the impact on our understanding of sources of reactive nitrogen deposition and the role of the nitrogen cycle on climate forcing.

Acknowledgments This work was supported by funding from the NASA GEO-CAPE Science Team. Although this work was reviewed by EPA and approved for publication, it may not necessarily reflect official agency policy. On behalf of all authors, the corresponding author states that there is no conflict of interest.

References

1. Abbatt JPD, Benz S, Cziczo DJ, Kanji Z, Lohmann U, Mohler O. Solid ammonium sulfate aerosols as ice nuclei: a pathway for cirrus cloud formation. Science. 2006;313:1770–3. doi:10.1126/Science.1129726.
2. Adams PJ, Seinfeld JH, Koch DM. Global concentrations of tropospheric sulfate, nitrate, and ammonium aerosol simulated in a general circulation model. J Geophys Res-Atmos. 1999;104:13 791–823.
3. Adams PJ, Seinfeld JH, Koch D, Mickley L, Jacob D. General circulation model assessment of direct radiative forcing by the sulfate-nitrate-ammonium-water inorganic aerosol system. J Geophys Res-Atmos. 2001;106:1097–111.
4. Aneja VP, Roelle PA, Murray GC, Southerland J, Erisman JW, Fowler D, et al. Atmospheric nitrogen compounds II: emissions, transport, transformation, deposition and assessment. Atmos Environ. 2001;35:1903–11. doi:10.1016/S1352-2310(00)00543-4.
5. Aneja VP, Schlesinger WH, Erisman JW, Behera SN, Sharma M, Battye W. Reactive nitrogen emissions from crop and livestock farming in India. Atmos Environ. 2012;47:92–103. doi:10.1016/J.Atmosenv.2011.11.026.
6. Asman WAH, Sutton MA, Schjorring JK. Ammonia: emission, atmospheric transport and deposition. New Phytol. 1998;139:27–48. doi:10.1046/J.1469-8137.1998.00180.X.
7. Athanasopoulou E, Tombrou M, Pandis SN, Russell AG. The role of sea-salt emissions and heterogeneous chemistry in the air quality of polluted coastal areas. Atmos Chem Phys. 2008;8:5755–69.
8. Aumann HH, Chahine MT, Gautier C, Goldberg MD, Kalnay E, McMillin LM, et al. AIRS/AMSU/HSB on the aqua mission: design, science objectives, data products, and processing systems. IEEE Trans Geosci Remote Sens. 2003;41:253–64. doi:10.1109/Tgrs.2002.808356.
9. Ball SM, Hanson DR, Eisele FL, McMurry PH. Laboratory studies of particle nucleation: initial results for H2SO4, H2O, and NH3 vapors. J Geophys Res-Atmos. 1999;104:23709–18. doi:10.1029/1999jd900411.
10. Bash JO, Cooter EJ, Dennis RL, Walker JT, Pleim JE. Evaluation of a regional air-quality model with bidirectional NH3 exchange coupled to an agroecosystem model. Biogeosciences. 2013;10:1635–45. doi:10.5194/Bg-10-1635-2013.
11. Bassett M, Seinfeld JH. Atmospheric equilibrium-model of sulfate and nitrate aerosols. Atmos Environ. 1983;17:2237–52. doi:10.1016/0004-6981(83)90221-4.
12. Battye W, Aneja VP, Roelle PA. Evaluation and improvement of ammonia emissions inventories. Atmos Environ. 2003;37:3873–83. doi:10.1016/S1352-2310(03)00343-1.
13. Bauer SE, Koch D, Unger N, Metzger SM, Shindell DT, Streets DG. Nitrate aerosols today and in 2030: a global simulation including aerosols and tropospheric ozone. Atmos Chem Phys. 2007;7:5043–59.
14. Beer R, Glavich TA, Rider DM. Tropospheric emission spectrometer for the earth observing system's Aura satellite. Appl Opt. 2001;40:2356–67. doi:10.1364/Ao.40.002356.
15. Beer R, Shephard MW, Kulawik S, Clough SA, Eldred RA, Bowman KW, et al. First satellite observations of lower tropospheric ammonia and methanol. Geophys Res Lett. 2008;35. doi:10.1029/2008GL033642.
16. Bell ML, Ebisu K, Peng RD, Samet JM, Dominici F. Hospital admissions and chemical composition of fine particle air pollution. Am J Resp Crit Care. 2009;179:1115–20. doi:10.1164/Rccm.200808-1240oc.
17. Bellouin N, Rae J, Jones A, Johnson C, Haywood J, Boucher O. Aerosol forcing in the Climate Model Intercomparison Project (CMIP5) simulations by HadGEM2-ES and the role of ammonium nitrate. J Geophys Res-Atmos. 2011;116:D20206. doi:10.1029/2011jd016074.
18. Bessagnet B, Beauchamp M, Guerreiro C, de Leeuw F, Tsyro S, Colette A, et al. Can further mitigation of ammonia emissions reduce exceedances of particulate matter air quality standards? Environ Sci Pol. 2014;44:149–63. doi:10.1016/J.Envsci.2014.07.011.
19. Beusen AHW, Bouwman AF, Heuberger PSC, Van Drecht G, Van Der Hoek KW. Bottom-up uncertainty estimates of global ammonia emissions from global agricultural production systems. Atmos Environ. 2008;42:6067–77.
20. Bones DL, Henricksen DK, Mang SA, Gonsior M, Bateman AP, Nguyen TB, et al. Appearance of strong absorbers and fluorophores in limonene-O-3 secondary organic aerosol due to NH4+-mediated chemical aging over long time scales. J Geophys Res-Atmos. 2010;115:D05203. doi:10.1029/2009jd012864.
21. Bouwman AF, Lee DS, Asman WAH, Dentener FJ, VanderHoek KW, Olivier JGJ. A global high-resolution emission inventory for ammonia. Glob Biogeochem Cycles. 1997;11:561–87.
22. Bouwman L, Goldewijk KK, Van Der Hoek KW, Beusen AHW, Van Vuuren DP, Willems J, et al. Exploring global changes in nitrogen and phosphorus cycles in agriculture induced by livestock production over the 1900–2050 period. Proc Natl Acad Sci USA. 2013;110:20882–7. doi:10.1073/Pnas.1012878108.
23. Brauer M, Amann M, Burnett RT, Cohen A, Dentener F, Ezzati M, et al. Exposure assessment for estimation of the global burden of disease attributable to outdoor air pollution. Environ Sci Technol. 2012;46:652–60.
24. Brook RD, Rajagopalan S, Pope CA, Brook JR, Bhatnagar A, Diez-Roux AV, et al. Particulate matter air pollution and cardiovascular disease an update to the scientific statement from the American Heart Association. Circulation. 2010;121:2331–78. doi:10.1161/Cir.0b013e3181dbece1.
25. Buonocore JJ, Dong XY, Spengler JD, Fu JS, Levy JI. Using the Community Multiscale Air Quality (CMAQ) model to estimate public health impacts of PM2.5 from individual power plants. Environ Int. 2014;68:200–8. doi:10.1016/J.Envint.2014.03.031.

26. Burnett RT, Brook J, Dann T, Delocla C, Philips O, Cakmak S, et al. Association between particulate- and gas-phase components of urban air pollution and daily mortality in eight Canadian cities. Inhal Toxicol. 2000;12:15–39. doi:10.1080/089583700750019495.
27. CAAC: Twelfth five-year plan on air pollution prevention and control in key regions, Tech. rep. 2013.
28. Carfrae JA, Sheppard LJ, Raven J, Stein W, Leith ID, Theobald A, et al. Early effects of atmospheric ammonia deposition on C alluna vulgaris (L.) hull growing on an ombrotrophic peat bog. Water Air Soil Pollut Focus. 2004;4:229–39.
29. Chen X, Day D, Schichtel B, Malm W, Matzoll AK, Mojica J, et al. Seasonal ambient ammonia and ammonium concentrations in a pilot IMPROVE NHx monitoring network in the western United States. Atmos Environ. 2014; 91:118–26.
30. Chuang CC, Penner JE, Taylor KE, Grossman AS, Walton JJ. An assessment of the radiative effects of anthropogenic sulfate. J Geophys Res-Atmos. 1997;102:3761–78. doi:10.1029/96jd03087.
31. Clarisse L, Clerbaux C, Dentener F, Hurtmans D, Coheur PF. Global ammonia distribution derived from infrared satellite observations. Nat Geosci. 2009;2:479–83.
32. Clarisse L, Shephard MW, Dentener F, Hurtmans D, Cady-Pereira K, Karagulian F, et al. Satellite monitoring of ammonia: a case study of the San Joaquin Valley. J Geophys Res-Atmos. 2010;115. doi:10.1029/2009jd013291.
33. Clerbaux C, Boynard A, Clarisse L, George M, Hadji-Lazaro J, Herbin H, et al. Monitoring of atmospheric composition using the thermal infrared IASI/MetOp sounder. Atmos Chem Phys. 2009;9:6041–54.
34. Cooter EJ, Bash JO, Walker JT, Jones MR, Robarge W. Estimation of NH_3 bidirectional flux from managed agricultural soils. Atmos Environ. 2010;44:2107–15. doi:10.1016/J.Atmosenv.2010.02.044.
35. Cooter EJ, Bash JO, Benson V, Ran L. Linking agricultural crop management and air quality models for regional to national-scale nitrogen assessments. Biogeosciences. 2012;9:4023–35. doi:10.5194/Bg-9-4023-2012.
36. Crouse DL, Peters PA, van Donkelaar A, Goldberg MS, Villeneuve PJ, Brion O, et al. Risk of non accidental and cardiovascular mortality in relation to long-term exposure to low concentrations of fine particulate matter: a canadian national-level cohort study. Environ Health Perspect. 2012; 120:708–14.
37. Dedoussi IC, Barrett SRH. Air pollution and early deaths in the United States. Part II: Attribution of PM2.5 exposure to emissions species, time, location and sector. Atmos Environ. 2014;99:610–17. doi:10.1016/J.Atmosenv.2014.10.033.
38. Delgado C, Rosegrant M, Steinfeld H, Ehui S, Courbois C. IFPRI food, agriculture, and the environment discussion paper 28. Washington, D.C. (USA): IFPRI. 1999.
39. Dennis RL, Mathur R, Pleim JE, Walker JT. Fate of ammonia emissions at the local to regional scale as simulated by the community multiscale air quality model. Atmos Pollut Res. 2010;1:207–14. doi:10.5094/Apr.2010.027.
40. Dennis RL, Schwede DB, Bash JO, Pleim JE, Walker JT, Foley KM. Sensitivity of continental United States atmospheric budgets of oxidized and reduced nitrogen to dry deposition parametrizations. Philos T R Soc B. 2013;368. doi:10.1098/Rstb.2013.0124.
41. Dentener F, Drevet J, Lamarque JF, Bey I, Eickhout B, Fiore AM, et al. Nitrogen and sulfur deposition on regional and global scales: a multimodel evaluation. Global Biogeochem Cycles. 2006;20:GB4003. doi:10.1029/2005GB002672.
42. Dentener FJ, Crutzen PJ. A 3-dimensional model of the global ammonia cycle. J Atmos Chem. 1994;19:331–69. doi:10.1007/Bf00694492.
43. Dupre C, Stevens CJ, Ranke T, Bleeker A, Peppler-Lisbach C, Gowing DJG, et al. Changes in species richness and composition in European acidic grasslands over the past 70 years: the contribution of cumulative atmospheric nitrogen deposition. Glob Chang Biol. 2010;16:344–57. doi:10.1111/J.1365-2486.2009.01982.X.
44. EEA: European Environment Agency: Ammonia (NH3) emissions (APE 003) Assessment, Tech. rep. 2014.
45. Ellis RA, Murphy JG, Pattey E, van Haarlem R, Obrien JM, Herndon SC. Characterizing a Quantum Cascade Tunable Infrared Laser Differential Absorption Spectrometer (QC-TILDAS) for measurements of atmospheric ammonia. Atmos Meas Tech. 2010;3:397–406.
46. Ellis RA, Murphy JG, Markovic MZ, VandenBoer TC, Makar PA, Brook J, et al. The influence of gas-particle partitioning and surface-atmosphere exchange on ammonia during BAQS-Met. Atmos Chem Phys. 2011;11: 133–45.
47. Ellis RA, Jacob DJ, Sulprizio MP, Zhang L, Holmes CD, Schichtel BA, et al. Present and future nitrogen deposition to national parks in the United States: critical load exceedances. Atmos Chem Phys. 2013;13:9083–95.
48. EPA: Integrated science assessment for particulate matter (final report). 2009.
49. Erisman JW, Sutton MA, Galloway J, Klimont Z, Winiwarter W. How a century of ammonia synthesis changed the world. Nat Geosci. 2008;1:636–9. doi:10.1038/Ngeo325.
50. Fann N, Fulcher CM, Hubbell BJ. The influence of location, source, and emission type in estimates of the human health benefits of reducing a ton of air pollution. Air Qual Atmos Health. 2009;2:169–76.
51. Fann N, Lamson AD, Anenberg SC, Wesson K, Risley D, Hubbell BJ. Estimating the National Public Health Burden Associated with Exposure to Ambient PM2.5 and Ozone. Risk Anal. 2012;32:81–95. doi:10.1111/J.1539-6924.2011.01630.X.
52. Fehsenfeld FC, Huey LG, Sueper DT, Norton RB, Williams EJ, Eisele FL, et al. Ground-based intercomparison of nitric acid measurement techniques. J Geophys Res-Atmos. 1998;103:3343–53. doi:10.1029/97jd02213.
53. Fehsenfeld FC, Huey LG, Leibrock E, Dissly R, Williams E, Ryerson TB, et al. Results from an informal intercomparison of ammonia measurement techniques. J Geophys Res-Atmos. 2002;107:4812. doi:10.1029/2001jd001327.
54. Feichter J, Lohmann U, Schult I. The atmospheric sulfur cycle in ECHAM-4 and its impact on the shortwave radiation. Clim Dynam. 1997;13:235–46. doi:10.1007/S003820050163.
55. Fishman J, Iraci LT, Al-Saadi J, Chance KV, Chavez F, Chin M, et al. The United States' next generation of atmospheric composition and coastal ecosystem measurements: NASA's Geostationary Coastal and Air Pollution Events (GEO-CAPE) mission. Bull Am Meteorol Soc. 2012;93:1547–66.
56. Flechard CR, Massad RS, Loubet B, Personne E, Simpson D, Bash JO, et al. Advances in understanding, models and parameterizations of biosphere-atmosphere ammonia exchange. Biogeosciences. 2013;10:5183–225. doi:10.5194/Bg-10-5183-2013.
57. Fowler D, Coyle M, Skiba U, Sutton MA, Cape JN, Reis S, et al. The global nitrogen cycle in the twenty-first century. Philos T R Soc B. 2013;368:20130164. doi:10.1098/Rstb.2013.0164.
58. Friedrich R, Reis S. Emissions of air pollutants: measurements, calculations and uncertainties, 978-3-662-07015-4. Berlin: Springer; 2004.

59. Fu X, Wang SX, Ran LM, Pleim JE, Cooter E, Bash JO, et al. Estimating NH_3 emissions from agricultural fertilizer application in China using the bidirectional CMAQ model coupled to an agro-ecosystem model. Atmos Chem Phys Discuss. 2015; 15:745–78.
60. Galloway JN, Aber JD, Erisman JW, Seitzinger SP, Howarth RW, Cowling EB, et al. The nitrogen cascade. Bioscience. 2003;53:341–56.
61. Galloway JN, Dentener FJ, Capone DG, Boyer EW, Howarth RW, Seitzinger SP, et al. Nitrogen cycles: past, present, and future. Biogeochemistry. 2004;70:153–226.
62. Galloway JN, Townsend AR, Erisman JW, Bekunda M, Cai ZC, Freney JR, et al. Transformation of the nitrogen cycle: recent trends, questions, and potential solutions. Science. 2008;320:889–92. doi:10.1126/Science.1136674.
63. Galloway JN, Leach AM, Bleeker A, Erisman JW. A chronology of human understanding of the nitrogen cycle. Philos T R Soc B. 2013;368. doi:10.1098/Rstb.2013.0120.
64. Galperin MV, Sofiev MA. The long-range transport of ammonia and ammonium in the Northern Hemisphere. Atmos Environ. 1998;32:373–80. doi:10.1016/S1352-2310(97)00045-9.
65. Gilliland AB, Dennis RL, Roselle SJ, Pierce TE. Seasonal NH_3 emission estimates for the eastern United States based on ammonium wet concentrations and an inverse modeling method. J Geophys Res-Atmos. 2003;108. doi:10.1029/2002JD003063.
66. Gilliland AB, Appel KW, Pinder RW, Dennis RL. Seasonal NH_3 emissions for the continental United States: inverse model estimation and evaluation. Atmos Environ. 2006;40:4986–98.
67. Ginoux P, Clarisse L, Clerbaux C, Coheur PF, Dubovik O, Hsu NC, et al. Mixing of dust and NH_3 observed globally over anthropogenic dust sources. Atmos Chem Phys. 2012;12:7351–63. doi:10.5194/Acp-12-7351-2012.
68. Gong LW, Lewicki R, Griffin RJ, Tittel FK, Lonsdale CR, Stevens RG, et al. Role of atmospheric ammonia in particulate matter formation in Houston during summertime. Atmos Environ. 2013;77:893–900. doi:10.1016/J.Atmosenv.2013.04.079.
69. Gu BJ, Ge Y, Ren Y, Xu B, Luo WD, Jiang H, et al. Atmospheric reactive nitrogen in China: sources, recent trends, and damage costs. Environ Sci Technol. 2012;46:9420–7. doi:10.1021/Es301446g.
70. Guo S, Hu M, Zamora ML, Peng JF, Shang DJ, Zheng J, et al. Elucidating severe urban haze formation in China. Proc Natl Acad Sci U S A. 2014;111:17373–8. doi:10.1073/Pnas.1419604111.
71. Hamaoui-Laguel L, Meleux F, Beekmann M, Bessagnet B, Genermont S, Cellier P, et al. Improving ammonia emissions in air quality modelling for France. Atmos Environ. 2014;92:584–95. doi:10.1016/J.Atmosenv.2012.08.002.
72. Hansen DA, Edgerton ES, Hartsell BE, Jansen JJ, Kandasamy N, Hidy GM, et al. The Southeastern aerosol research and characterization study: part 1-overview. J Air Waste Manage Assoc. 2003;53:1460–71.
73. Hauglustaine DA, Balkanski Y, Schulz M. A global model simulation of present and future nitrate aerosols and their direct radiative forcing of climate. Atmos Chem Phys. 2014;14:11031–63. doi:10.5194/Acp-14-11031-2014.
74. Haywood JM, Shine KP. The effect of anthropogenic sulfate and soot aerosol on the clear-sky planetary radiation budget. Geophys Res Lett. 1995;22:603–6. doi:10.1029/95gl00075.
75. Haywood JM, Roberts DL, Slingo A, Edwards JM, Shine KP. General circulation model calculations of the direct radiative forcing by anthropogenic sulfate and fossil-fuel soot aerosol. J Climate. 1997;10:1562–77. doi:10.1175/1520-0442(1997)010<1562:Gcmcot>2.0.Co;2.
76. Heald CL, Collet JL, Lee T, Benedict KB, Schwandner FM, Li Y, et al. Atmospheric ammonia and particulate inorganic nitrogen over the United States. Atmos. Chem. Phys. 2012;12:10295–312. doi:10.5194/acp-12-10295-2012.
77. Henze DK, Seinfeld JH, Shindell D. Inverse modeling and mapping U.S. air quality influences of inorganic $PM_{2.5}$ precursor emissions using the adjoint of GEOS-Chem. Atmos Chem Phys. 2009;9:5877–903.
78. Henze DK, Shindell DT, Akhtar F, Spurr RJD, Pinder RW, Loughlin D, et al. Spatially refined aerosol direct radiative forcing efficiencies. Environ Sci Technol. 2012;46:9511–8. doi:10.1021/es301993s.
79. Huang X, Song Y, Li MM, Li JF, Huo Q, Cai XH, et al. A high-resolution ammonia emission inventory in China. Global Biogeochem Cycles. 2012;26:Gb1030. doi:10.1029/2011gb004161.
80. Huey LG, Dunlea EJ, Lovejoy ER, Hanson DR, Norton, RB, Fehsenfeld FC, et al. Fast time response measurements of HNO3 in air with a chemical ionization mass spectrometer. J Geophys Res-Atmos;103:3355–60. doi:10.1029/97jd02214.
81. Huntzicker JJ, Cary RA, Ling CS. Neutralization of sulfuric-acid aerosol by ammonia. Environ Sci Technol. 1980;14:819–24. doi:10.1021/Es60167a009.
82. Iinuma Y, Boge O, Gnauk T, Herrmann H. Aerosol-chamber study of the alpha-pinene/O-3 reaction: influence of particle acidity on aerosol yields and products. Atmos Environ. 2004;38:761–73. doi:10.1016/J.Atmosenv.2003.10.015.
83. Jacobson MZ. Global direct radiative forcing due to multicomponent anthropogenic and natural aerosols. J Geophys Res-Atmos. 2001;106:1551–68.
84. Jones L, Provins A, Holland M, Mills G, Hayes F, Emmett B, et al. A review and application of the evidence for nitrogen impacts on ecosystem services. Ecosyst Serv. 2014;7:76–88. doi:10.1016/j.ecoser.2013.09.001.
85. Kelley J, Baker KR, Nowak JB, Murphy JG, Markovic MZ, VandenBoer TC, et al. Fine-scale simulation of ammonium and nitrate over the South Coast Air Basin and San Joaquin Valley of California during CalNex-2010. J Geophys Res-Atmos. 2014;119:3600–14. doi:10.1002/2013JD021290.
86. Kharol SK, Martin RV, Philip S, Vogel S, Henze DK, Chen D, et al. Persistent sensitivity of Asian aerosol to emissions of nitrogen oxides. Geophys Res Lett. 2013;40:1021–6. doi:10.1002/Grl.50234.
87. Kim YP, Seinfeld JH, Saxena P. Atmoshperic gas-aerosol equilibrium—I. Thermodynamic Model. Aerosol Sci Tech. 1993a;19:157–81.
88. Kim YP, Seinfeld JH, Saxena P. Atmoshperic gas-aerosol equilibrium—II. Analysis of common approximations and activity coefficient calculation methods. Aerosol Sci Tech. 1993b;19:182–98.
89. Kirkby J, Curtius J, Almeida J, Dunne E, Duplissy J, Ehrhart S, et al. Role of sulphuric acid, ammonia and galactic cosmic rays in atmospheric aerosol nucleation. Nature. 2011;476:429–U77. doi:10.1038/Nature10343.
90. Koo B, Piyachaturawat P, Morris R, Knipping EM. Evaluation of the variability in chemical transport model performance for deposition and ambient concentrations of nitrogen and sulfur compounds. Atmosphere. 2012;3: 400–18.
91. Kruit RJW, Schaap M, Sauter FJ, van Zanten MC, van Pul WAJ. Modeling the distribution of ammonia across Europe including bidirectional surface-atmosphere exchange. Biogeosciences. 2012;9:5261–77. doi:10.5194/Bg-9-5261-2012.

92. Krupa SV. Effects of atmospheric ammonia (NH3) on terrestrial vegetation: a review. Environ Pollut. 2003;124:179–221. doi:10.1016/S0269-7491(02)00434-7.
93. Kulmala M, Korhonen P, Napari I, Karlsson A, Berresheim H, O'Dowd CD. Aerosol formation during PARFORCE: ternary nucleation of H2SO4, NH3, and H2O. J Geophys Res-Atmos. 2002;107:8111. doi:10.1029/2001jd000900.
94. Lamarque JF, Kyle G, Meinshausen M, Riahi K, Smith S, van Vuuren D, et al. Global and regional evolution of short-lived radiatively-active gases and aerosols in the representative concentration pathways. Clim Chang. 2011;109:191–212.
95. Langridge JM, Lack D, Brock CA, Bahreini R, Middlebrook AM, Neuman JA, et al. Evolution of aerosol properties impacting visibility and direct climate forcing in an ammonia-rich urban environment. J Geophys Res-Atmos. 2012;117:D00v11. doi:10.1029/2011jd017116.
96. Lee AKY, Zhao R, Li R, Liggio J, Li SM, Abbatt JPD. Formation of light absorbing organo-nitrogen species from evaporation of droplets containing glyoxal and ammonium sulfate. Environ Sci Technol. 2013;47:12819–26. doi:10.1021/Es402687w.
97. Lee CJ, Martin RV, Henze DK, Brauer M, Cohen A, Donkelaar, AV. Response of global particulate-matter-related mortality to changes in local precursor emissions. Environ Sci Technol. 2015;49(7):4335–44. doi:10.1021/acs.est.5b00873.
98. Lepeule J, Laden F, Dockery D, Schwartz J. Chronic exposure to fine particles and mortality: an extended follow-up of the Harvard six cities study from 1974 to 2009. Environ Health Perspect. 2012;120:965–70. doi:10.1289/Ehp.1104660.
99. Levy JI, Diez D, Dou YP, Barr CD, Dominici F. A meta-analysis and multisite time-series analysis of the differential toxicity of major fine particulate matter constituents. Am J Epidemiol. 2012;175:1091–9. doi:10.1093/Aje/Kwr457.
100. Li Y, Schwandner FM, Sewell HJ, Zivkovich A, Tigges M, Raja S, et al. Observations of ammonia, nitric acid, and fine particles in a rural gas production region. Atmos Environ. 2014;83:80–9.
101. Liao H, Seinfeld JH. Global impacts of gas-phase chemistry-aerosol interactions on direct radiative forcing by anthropogenic aerosols and ozone. J Geophys Res-Atmos. 2005;110. doi:10.1029/2005JD005907.
102. Liggio J, Li SM, Vlasenko A, Stroud C, Makar P. Depression of ammonia uptake to sulfuric acid aerosols by competing uptake of ambient organic gases. Environ Sci Technol. 2011;45:2790–6. doi:10.1021/Es103801g.
103. Lim SS, Vos T, Flaxman AD, Danaei G, Shibuya K, Adair-Rohani H, et al. A comparative risk assessment of burden of disease and injury attributable to 67 risk factors and risk factor clusters in 21 regions, 1990–2010: a systematic analysis for the Global Burden of Disease Study 2010. Lancet. 2012;380:2224–60.
104. Lin YH, Knipping EM, Edgerton ES, Shaw SL, Surratt JD. Investigating the influences of SO_2 and NH_3 levels on isoprene-derived secondary organic aerosol formation using conditional sampling approaches. Atmos Chem Phys. 2013;13:8457–70. doi:10.5194/Acp-13-8457-2013.
105. Liu X, Zhang Y, Han W, Tang A, Shen J, Cui Z, et al. Enhanced nitrogen deposition over China. Nature. 2013;494:459–62.
106. Liu Y, Liggio J, Staebler R, Li SM. Reactive uptake of ammonia to secondary organic aerosols: kinetics of organonitrogen formation. Atmos Chem Phys Discuss. 2015;15:17449–90. doi:10.5194/acpd-15-17449-2015.
107. Luo M, Shephard MW, Cady-Pereira KE, Henze DK, Zhu L, Bash JO, et al. Satellite observations of tropospheric ammonia and carbon monoxide: global distributions, correlations and comparisons to model simulations. Atmos Environ. 2015;106:262–77. doi:10.1016/j.atmosenv.2015.02.007.
108. Malm WC, Schichtel BA, Barna MG, Gebhart KA, Rodriguez MA, Collett JL, et al. Aerosol species concentrations and source apportionment of ammonia at Rocky Mountain National Park. J Air Waste Manage Assoc. 2013;63:1245–63.
109. Martin ST, Hung HM, Park RJ, Jacob DJ, Spurr RJD, Chance KV, et al. Effects of the physical state of tropospheric ammonium-sulfate- nitrate particles on global aerosol direct radiative forcing. Atmos Chem Phys. 2004;4:183–214.
110. Massad RS, Nemitz E, Sutton MA. Review and parameterisation of bidirectional ammonia exchange between vegetation and the atmosphere. Atmos Chem Phys. 2010;10:10 359–86. doi:10.5194/Acp-10-10359-2010.
111. Miller DJ, Sun K, Tao L, Khan MA, Zondlo MA. Open-path, quantum cascade-laser-based sensor for high-resolution atmospheric ammonia measurements. Atmos Meas Tech. 2014;7:81–93.
112. Morgan WT, Allan JD, Bower KN, Esselborn M, Harris B, Henzing JS, et al. Enhancement of the aerosol direct radiative effect by semi-volatile aerosol components: airborne measurements in North-Western Europe. Atmos Chem Phys. 2010;10:8151–71. doi:10.5194/Acp-10-8151-2010.
113. Moss RH, Edmonds JA, Hibbard KA, Manning MR, Rose SK, van Vuuren DP, et al. The next generation of scenarios for climate change research and assessment. Nature. 2010;463:747–56.
114. Myhre G, Berglen TF, Johnsrud M, Hoyle CR, Berntsen TK, Christopher SA, et al. Modelled radiative forcing of the direct aerosol effect with multi-observation evaluation. Atmos Chem Phys. 2009;9:1365–92. doi:10.5194/Acp-9-1365-2009.
115. Myhre G, Shindell D, Breon FM, Collins B, Fuglestvedt J, Huang J, et al. Anthropogenic and natural radiative forcing. 2013. Tech. rep.
116. Na K, Song C, Switzer C, Cocker DR. Effect of ammonia on secondary organic aerosol formation from alpha-Pinene ozonolysis in dry and humid conditions. Environ Sci Technol. 2007;41:6096–102. doi:10.1021/Es061956y.
117. Napari I, Kulmala M, Vehkamaki H. Ternary nucleation of inorganic acids, ammonia, and water. J Chem Phys. 2002;117:8418–25. doi:10.1063/1.1511722.
118. Nemitz E, Sutton MA, Schjoerring JK, Husted S, Wyers GP. Resistance modelling of ammonia exchange over oilseed rape. Agric For Meteorol. 2000;105:405–25. doi:10.1016/S0168-1923(00)00206-9.
119. Nenes A, Pandis SN, Pilinis C. ISORROPIA: a new thermodynamic equilibrium model for multiphase multicomponent inorganic aerosols. Aquat Geochem. 1998;4:123–52.
120. Norman M, Spirig C, Wolff V, Trebs I, Flechard C, Wisthaler A, et al. Intercomparison of ammonia measurement techniques at an intensively managed grassland site (Oensingen, Switzerland). Atmos Chem Phys. 2009;9:2635–45.
121. Nowak JB, Huey LG, Russell AG, Tian D, Neuman JA, Orsini D, et al. Analysis of urban gas phase ammonia measurements from the 2002 Atlanta Aerosol Nucleation and Real-Time Characterization Experiment (ANARChE). J Geophys Res-Atmos. 2006;111. doi:10.1029/2006JD007113.
122. Nowak JB, Neuman JA, Kozai K, Huey LG, Tanner DJ, Holloway JS, et al. A chemical ionization mass spectrometry technique for airborne measurements of ammonia. J Geophys Res-Atmos. 2007:112.

123. Nowak JB, Neuman JA, Bahreini R, Brock CA, Middlebrook AM, Wollny AG, et al. Airborne observations of ammonia and ammonium nitrate formation over Houston, Texas. J Geophys Res-Atmos (1984–2012). 2010;115:D22 304.
124. Nowak JB, Neuman JA, Bahreini R, Middlebrook AM, Holloway JS, McKeen SA, et al. Ammonia sources in the California South Coast Air Basin and their impact on ammonium nitrate formation. Geophys Res Lett. 2012:39.
125. NRC: Earth Science and Applications from Space: national imperatives for the next decade and beyond. Washington: The National Academies Press. 2007.
126. Paerl HW, Dennis RL, Whitall DR. Atmospheric deposition of nitrogen: implications for nutrient overenrichment of coastal waters. Estuaries. 2002;24:667–93.
127. Park RJ, Jacob D, Field BD, Yantosca R, Chin M. Natural and transboundary pollution influences on sulfate-nitrate-ammonium aerosols in the United States: implications for policy. J Geophys Res-Atmos. 2004;109. doi:10.1029/2003JD004473.
128. Paulot F, Jacob DJ. Hidden cost of U.S. agricultural exports: particulate matter from ammonia emissions. Environ Sci Technol. 2014;48:903–8. doi:10.1021/Es4034793.
129. Paulot F, Jacob DJ, Henze DK. Sources and processes contributing to nitrogen deposition: an adjoint model analysis applied to biodiversity hotspots worldwide. Environ Sci Technol. 2013;47:3226–33. doi:10.1021/Es3027727.
130. Paulot F, Jacob DJ, Pinder RW, Bash JO, Travis K, Henze DK. Ammonia emissions in the United States, European Union, and China derived by high-resolution inversion of ammonium wet deposition data: interpretation with a new agricultural emissions inventory (MASAGE_NH3). J Geophys Res-Atmos. 2014;119:4343--64. doi:10.1002/2013jd021130.
131. Philip S, Martin RV, van Donkelaar A, Wai-Ho L, Wang Y, Chen D, et al. Global chemical composition of ambient fine particulate matter estimated from satellite observations and a chemical transport model. Environ Sci Technol. 2014;48:13060–8. doi:10.1021/es502965b.
132. Phoenix GK, Emmett BA, Britton AJ, Caporn SJM, Dise NB, Helliwell R, et al. Impacts of atmospheric nitrogen deposition: responses of multiple plant and soil parameters across contrasting ecosystems in long-term field experiments. Glob Chang Biol. 2012;18:1197–215. doi:10.1111/J.1365-2486.2011.02590.X.
133. Pinder RW, Pekney NJ, Davidson CI, Adams PJ. A process-based model of ammonia emissions from dairy cows: improved temporal and spatial resolution. Atmos Environ. 2004;38:1357–65.
134. Pinder RW, Adams PJ, Pandis SN, Gilliland AB. Temporally resolved ammonia emission inventories: current estimates, evaluation tools, and measurement needs. J Geophys Res-Atmos. 2006;111. doi:10.1029/2005JD006603.
135. Pinder RW, Adams PJ, Pandis SN. Ammonia emission controls as a cost-effective strategy for reducing atmospheric particulate matter in the eastern United States. Environ Sci Technol. 2007;41:380–6.
136. Pinder RW, Walker JT, Bash JO, Cady-Pereira KE, Henze DK, Luo M, et al. Quantifying spatial and temporal variability in atmospheric ammonia with in situ and space-based observations. Geophys Res Lett. 2011;38:L04 802. doi:10.1029/2010GL046146.
137. Pinder RW, Davidson EA, Goodale CL, Greaver TL, Herrick JD, Liu LL. Climate change impacts of US reactive nitrogen. Proc Natl Acad Sci U S A. 2012;109:7671–5. doi:10.1073/Pnas.1114243109.
138. Pinder RW, Bettez ND, Bonan GB, Greaver TL, Wieder WR, Schlesinger WH, et al. Impacts of human alteration of the nitrogen cycle in the US on radiative forcing. Biogeochemistry. 2013;114:25–40. doi:10.1007/S10533-012-9787-Z.
139. Pleim JE, Bash JO, Walker JT, Cooter EJ. Development and evaluation of an ammonia bidirectional flux parameterization for air quality models. J Geophys Res Atmos. 2013;118. doi:10.1002/jgrd.50262.
140. Pope CA, Burnett RT, Thun MJ, Calle EE, Krewski D, Ito K, et al. Lung cancer, cardiopulmonary mortality, and long-term exposure to fine particulate air pollution. J Am Med Assoc. 2002;287:1132–41.
141. Pope CA, Ezzati M, Dockery DW. Fine-particulate air pollution and life expectancy in the United States. N Engl J Med. 2009;360(4):376–86.
142. Prather M, Flato G, Friedlingstein P, Jones C, Lamarque JF, Liao H, et al. IPCC, 2013: Annex II: climate system scenario tables, in climate change 2013. 2013.
143. Puchalski MA, Sather ME, Walker JT, Lelunann CMB, Gay DA, Mathew J, et al. Passive ammonia monitoring in the United States: comparing three different sampling devices. J Environ Monit. 2011;13:3156–67.
144. Puchalski MA, Rogers CM, Baumgardner R, Mishoe KP, Price G, Smith MJ, et al. A statistical comparison of active and passive ammonia measurements collected at Clean Air Status and Trends Network (CASTNET) sites. Environmental Science: Processes & Impacts. 2015;17:358–69.
145. Reay DS, Dentener F, Smith P, Grace J, Feely RA. Global nitrogen deposition and carbon sinks. Nat Geosci. 2008;1:430–7. doi:10.1038/Ngeo230.
146. Reiss R, Anderson EL, Cross CE, Hidy G, Hoel D, McClellan R, et al. Evidence of health impacts of sulfate- and nitrate-containing particles in ambient air. Inhal Toxicol. 2007;19:419–49. doi:10.1080/08958370601174941.
147. R'honi Y, Clarisse L, Clerbaux C, Hurtmans D, Duflot V, Turquety S, et al. Exceptional emissions of NH_3 and HCOOH in the 2010 Russian wildfires. Atmos Chem Phys. 2013;13:4171–81. doi:10.5194/Acp-13-4171-2013.
148. Riddick SN, Dragosits U, Blackall TD, Daunt F, Wanless S, Sutton MA. The global distribution of ammonia emissions from seabird colonies. Atmos Environ. 2012;55:319–27. doi:10.1016/J.Atmosenv.2012.02.052.
149. Roe SM, Spivey MD, Lindquist HC, Thesing KB, Strait RP, Pechan EH. Estimating ammonia emissions from anthropogenic nonagricultural sources, Tech. rep. 2004.
150. Saylor RD, Edgerton ES, Hartsell BE, Baumann K, Hansen DA. Continuous gaseous and total ammonia measurements from the southeastern aerosol research and characterization (SEARCH) study. Atmos Environ. 2010;44:4994–5004.
151. Schlesinger WH. On the fate of anthropogenic nitrogen. Proc Natl Acad Sci USA. 2009;106:203–8. doi:10.1073/Pnas.0810193105.
152. Schlesinger WH, Hartley AE. A global budget for atmospheric NH_3. Biogeochemistry. 1992;15:191–211.
153. Schwartz J, Laden F, Zanobetti A. The concentration-response relation between $PM_{2.5}$ and daily deaths. Environ Health Perspect. 2002;110:1025–9.
154. Shephard MW, McLinden C, Cady-Pereira KE, Luo M, Moussa SG, Leithead A, et al. Satellite validation of ammonia, methanol, and formic acid over the canadian oil sands. 2015. submitted.
155. Shephard MW, Cady-Pereira KE. Cross-track Infrared Sounder (CrIS) satellite observations of tropospheric ammonia. Atmos Meas Tech Discuss. 2015;7:11 379–413.

156. Shephard MW, Worden HM, Cady-Pereira KE, Lampel M, Luo MZ, Bowman KW, et al. Tropospheric emission spectrometer nadir spectral radiance comparisons. J Geophys Res-Atmos. 2008;113. doi:10.1029/2007jd008856.
157. Shephard MW, Cady-Pereira KE, Luo M, Henze DK, Pinder RW, Walker JT, et al. TES ammonia retrieval strategy and global observations of the spatial and seasonal variability of ammonia. Atmos Chem Phys. 2011;11:10743–63.
158. Shindell DT, Faluvegi G, Koch DM, Schmidt GA, Unger N, Bauer SE. Improved attribution of climate forcing to emissions. Science. 2009;326:716–8. doi:10.1126/Science.1174760.
159. Shindell DT, Lamarque JF, Schulz M, Flanner M, Jiao C, Chin M, et al. Radiative forcing in the ACCMIP historical and future climate simulations. Atmos Chem Phys. 2013;13:2939–74. doi:10.5194/Acp-13-2939-2013.
160. Skjoth CA, Geels C. The effect of climate and climate change on ammonia emissions in Europe. Atmos Chem Phys. 2013;13:117–28. doi:10.5194/Acp-13-117-2013.
161. Skjoth CA, Geels C, Berge H, Gyldenkaerne S, Fagerli H, Ellermann T, et al. Spatial and temporal variations in ammonia emissions—a freely accessible model code for Europe. Atmos Chem Phys. 2011;11:5221–36. doi:10.5194/Acp-11-5221-2011.
162. Smith JN, Moore KF, Eisele FL, Voisin D, Ghimire AK, Sakurai H, et al. Chemical composition of atmospheric nanoparticles during nucleation events in Atlanta. J Geophys Res-Atmos. 2005;110:D22s03. doi:10.1029/2005jd005912.
163. Smith SJ, Bond TC. Two hundred fifty years of aerosols and climate: the end of the age of aerosols. Atmos Chem Phys. 2014;14:537–49. doi:10.5194/Acp-14-537-2014.
164. Sorooshian A, Murphy SN, Hersey S, Gates H, Padro LT, Nenes A, et al. Comprehensive airborne characterization of aerosol from a major bovine source. Atmos Chem Phys. 2008;8:5489–520.
165. Streets DG, Bond TC, Carmichael GR, Fernandes SD, Fu Q, He D, et al. An inventory of gaseous and primary aerosol emissions in Asia in the year 2000. J Geophys Res-Atmos. 2003;108. doi:10.1029/2002jd003093.
166. Sun K, Cady-Pereira K, Miller DJ, Tao L, Zondlo MA, Nowak JB, et al. Validation of TES ammonia observations at the single pixel scale in the San Joaquin Valley during DISCOVER-AQ. J Geophys Res. 2015;120. doi:10.1002/2014JD022846.
167. Sutton MA, Oenema O, Erisman JW, Leip A, van Grinsven H, Winiwarter W. Too much of a good thing. Nature. 2011b;472:159–61. doi:10.1038/472159a.
168. Sutton et al. The European nitrogen assessment. Cambridge: Cambridge University Press; 2011a.
169. Sutton MA, Reis S, Riddick SN, Dragosits U, Nemitz E, Theobald MR, et al. Towards a climate-dependent paradigm of ammonia emission and deposition. Philos T R Soc B. 2013;368:20130166. doi:10.1098/Rstb.2013.0166.
170. Tobin DC, Revercomb HE, Knuteson RO, Best FA, Smith WL, Ciganovich NN, et al. Radiometric and spectral validation of atmospheric infrared sounder observations with the aircraft-based scanning high-resolution interferometer sounder. J Geophys Res-Atmos. 2006;111:D09s02. doi:10.1029/2005jd006094.
171. Updyke KM, Nguyen TB, Nizkorodov SA. Formation of brown carbon via reactions of ammonia with secondary organic aerosols from biogenic and anthropogenic precursors. Atmos Environ. 2012;63:22–31. doi:10.1016/J.Atmosenv.2012.09.012.
172. Van Damme M, Clarisse L, Heald CL, Hurtmans D, Ngadi Y, Clerbaux C, et al. Global distributions, time series and error characterization of atmospheric ammonia (NH3) from IASI satellite observations. Atmos Chem Phys. 2014;14:2905–22. doi:10.5194/Acp-14-2905-2014.
173. Van Damme M, Clarisse L, Dammers E, Liu X, Nowak JB, Clerbaux C, et al. Towards validation of ammonia (NH_3) measurements from the IASI satellite. Atmos. Meas. Tech. 2015;8:1575–91. doi:10.5194/amt-8-1575-2015.
174. van Donkelaar A, Martin RV, Leaitch WR, Macdonald AM, Walker TW, Streets DG, et al. Analysis of aircraft and satellite measurements from the intercontinental chemical transport experiment (INTEX-B) to quantify long-range transport of East Asian Sulfur to Canada. Atmos Chem Phys. 2008;8:2999–3014.
175. Vayenas DV, Takahama S, Davidson CI, Pandis SN. Simulation of the thermodynamics and removal processes in the sulfate-ammonia-nitric acid system during winter: implications for $PM_{2.5}$ control strategies. J Geophys Res-Atmos. 2005;110. doi:10.1029/2004JD005038.
176. Vitousek PM, Aber JD, Howarth RW, Likens GE, Matson PA, Schindler DW, et al. Human alteration of the global nitrogen cycle: sources and consequences. Ecol Appl. 1997;7:737–50. doi:10.2307/2269431.
177. von Bobrutzki K, Braban CF, Famulari D, Jones SK, Blackall T, Smith TEL, et al. Field inter-comparison of eleven atmospheric ammonia measurement techniques. Atmos Meas Tech. 2010;3:91–112. doi:10.5194/Amt-3-91-2010.
178. Wagstrom KM, Pandis SN. Source-receptor relationships for fine particulate matter concentrations in the Eastern United States. Atmos Environ. 2011;45:347–56. doi:10.1016/J.Atmosenv.2010.10.019.
179. Walker JM, Philip S, Martin RV, Seinfeld JH. Simulation of nitrate, sulfate, and ammonium aerosols over the United States. Atmos Chem Phys. 2012;12:11213–27. doi:10.5194/Acp-12-11213-2012.
180. Wang J, Hoffmann AA, Park RJ, Jacob DJ, Martin ST. Global distribution of solid and aqueous sulfate aerosols: effect of the hysteresis of particle phase transitions. J Geophys Res-Atmos. 2008a;113. doi:10.1029/2007jd009367.
181. Wang J, Jacob DJ, Martin ST. Sensitivity of sulfate direct climate forcing to the hysteresis of particle phase transitions. J Geophys Res-Atmos. 2008b;113. doi:10.1029/2007jd009368.
182. Wesely ML. Parameterization of surface resistances to gaseous dry deposition in regional-scale numerical-models. Atmos Environ. 1989;23:1293–304.
183. West JJ, Pilinis C, Nenes A, Pandis SN. Marginal direct climate forcing by atmospheric aerosols. Atmos Environ. 1998;32:2531–42.
184. West JJ, Ansari AS, Pandis SN. Marginal $PM_{2.5}$: nonlinear aerosol mass response to sulfate reductions in the Eastern United States. J Air Waste Manage Assoc. 1999;49:1415–24.
185. Worden H, Beer R, Bowman KW, Fisher B, Luo M, Rider D, et al. TES level 1 algorithms: interferogram processing, geolocation, radiometric, and spectral calibration. IEEE Trans Geosci Remote Sens. 2006;44:1288–96. doi:10.1109/Tgrs.2005.863717.
186. Xu L, Penner JE. Global simulations of nitrate and ammonium aerosols and their radiative effects. Atmos Chem Phys. 2012;12:9479–504. doi:10.5194/Acp-12-9479-2012.
187. Zhang L, Jacob DJ, Knipping EM, Kumar N, Munger JW, Carouge CC, et al. Nitrogen deposition to the United States: distribution, sources, and processes. Atmos Chem Phys. 2012;12:4539–54. doi:10.5194/Acp-12-4539-2012.
188. Zhang Q, Jimenez JL, Canagaratna MR, Ulbrich IM, Ng NL, Worsnop DR, et al. Understanding atmospheric organic aerosols via factor analysis of aerosol mass spectrometry: a review. Anal Bioanal Chem. 2011;401:3045–67. doi:10.1007/S00216-011-5355-Y.

189. Zhou Y, Cheng S, Lang J, Chen D, Zhao B, Liu C, et al. A comprehensive ammonia emission inventory with high-resolution and its evaluation in the Beijing-Tianjin-Hebei (BTH) region, China. Atmos Environ. 2015;106:305–17.
190. Zhu L, Henze DK, Cady-Pereira KE, Shephard MW, Luo M, Pinder RW, et al. Constraining U.S. ammonia emissions using TES remote sensing observations and the GEOS-Chem adjoint model. J Geophys Res-Atmos. 2013;118:3355–68. doi:10.1002/Jgrd.50166.
191. Zhu L, Henze DK, Bash JO, Jeong GR, Cady-Pereira KE, Shephard MW, et al. Global evaluation of ammonia bidirectional exchange. Atmos Chem Phys Discuss. 2015;15:4823–77.